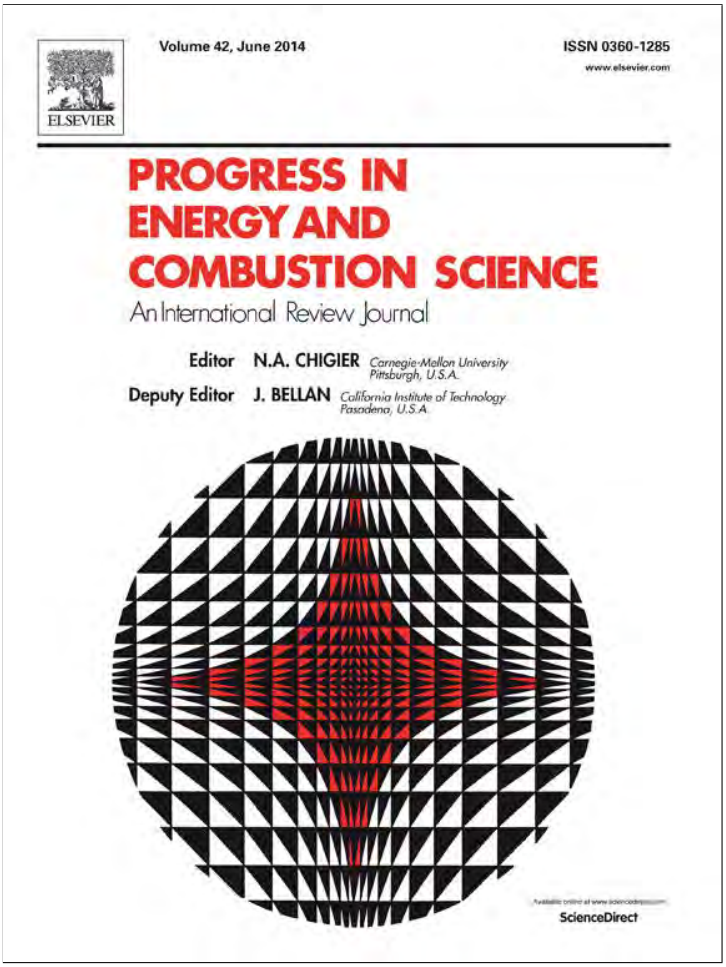

Progress in Energy and Combustion Science 42 (2014) 54–86

Contents lists available at ScienceDirect

Progress in Energy and Combustion Science

journal homepage: www.elsevier.com/locate/pecs

Review

Advances in droplet array combustion theory and modeling

William A. Sirignano*

Department of Mechanical and Aerospace Engineering, University of California, 3202 Engineering Gateway, Irvine, CA 92697-3975, USA

ARTICLE INFO

Article history:
Received 30 August 2013
Accepted 20 January 2014
Available online 15 February 2014

Keywords:
Multicomponent
Transient vaporization/heating
Droplet arrays

ABSTRACT

A review of research on the subject of the vaporization and burning of fuel droplets configured in a prescribed array is presented, including both classical works and research over the past decade or two. Droplet arrays and groups and the relation to sprays are discussed. The classical works are reviewed. Recent research on transient burning and vaporization of finite arrays with Stefan convection but without forced convection is presented, including extensions to non-unitary Lewis number and multi-component, liquid fuels. Recent results on transient, convective burning of droplets in arrays are also examined. In particular, transient convective burning of infinite (single-layer periodic and double-layer periodic) and finite droplet arrays are discussed; attention is given to the effects of droplet deceleration due to aerodynamic drag, diameter decrease due to vaporization, internal liquid circulation, and arrays with moving droplets in tandem and staggered configurations. Flame structure is examined as a function of spacing between neighboring droplets and Damköhler number: individual droplet flames versus group flames and wake flames versus envelope flames. Based on existing knowledge of laminar droplet array and spray combustion theory, experimental evidence, and turbulent studies for non-vaporizing and non-reacting two-phase flows, comments are made on the needs and implications for the study of turbulent spray and array combustion.

Contents

* Tel.: +1 949 824 3700; fax: +1 949 824 3773.
E-mail address: sirignan@uci.edu.

0360-1285/$ – see front matter © 2014 Elsevier Ltd. All rights reserved.
http://dx.doi.org/10.1016/j.pecs.2014.01.002

Nomenclature

Latin letters

a	droplet radius in Figs. 7 and 8
B_M	spalding mass transfer number
B_H	spalding heat transfer number
C_D	drag coefficient
C_L	lift coefficient
c_p	constant pressure specific heat
D	diffusion coefficient
d	droplet diameter, also droplet spacing in Figs. 7 and 8
Da	Damkohler number
E_a	activation energy
h	specific enthalpy
k	turbulence kinetic energy per unit mass
L	latent heat of vaporization
L_{eff}	effective latent heat of vaporization
Le	Lewis number
M	molecular weight
$\dot{m}$	mass vaporization rate
N	number of droplets or mole number
Nu	Nusselt number
p	pressure
Pr	Prandtl number
$\dot{q}$	magnitude of heat flux
Q	heat of combustion
r	radial coordinate
R	droplet radius or universal gas constant
Re	Reynolds number
Re_0	initial Reynolds number
Re_m	modified Reynolds number, defined after Eq. (35)
s	droplet spacing
S	stoichiometric number
Sc	Schmidt number
Sh	Sherwood number
sp	droplet spacing
T	temperature
T_b	boiling temperature
t	time
U_d	velocity of the droplet
U'_∞	relative velocity between the air stream and the droplet
u	velocity
V_A	array volume
V_l	total liquid volume in array
$\overrightarrow{V}$	mass-averaged velocity vector
W	molecular weight
We	Weber number
X	mole fraction
Y	mass fraction
1	unit tensor

Greek letters

α	thermal diffusivity
ε	mass flux fraction; also, turbulence kinetic energy dissipation rate
ζ	normalized radial coordinate
η_A	interactive-isolated vaporization ratio
θ	liquid volume fraction
λ	thermal conductivity
ν	stoichiometric mass ratio, fuel-to-oxidizer
ρ	density
τ_K	Kolmogorov time scale
τ_p	particle response time
ϕ	potential function
Φ	normalized potential function
σ_0	ratio of initial vortex radius to initial droplet radius
ξ	similarity parameter

Subscripts

avg	average value
eff	effective value
F	fuel vapor
film	film conditions (average of ambient and surface conditions)
g	gas phase
i	the ith species
iso	isolated droplet
j	integer index designating individual droplet in an array
l	liquid phase
lS	liquid surface
n	the nth species
O	oxygen
S	surface value
s	surface value
∞	ambient value
ε	mass-flux-averaged value
0	initial value

Superscript

$\hat{}$	average over gas phase
$\cdot$	dimensionless quantities
o	reference value

1. Introduction

The fuel-droplet and fuel-spray combustion literature has many research works addressing experimental and theoretical configurations where individual droplets are surrounded by their individual flames [1]. Yet, observers of practical spray flames find many droplets engulfed by a closed flame. Chigier and McCreath [2] observed such engulfment in the laboratory. More recently, Candel et al. [3] also found evidence that a thick flame shell surrounds portions of the spray. In this review, there will be a focus on a certain theoretical approach to understanding this phenomenon and the interactions amongst vaporizing droplets in a spray flame.

There are various classes of configurations where a collection of interactive vaporizing and burning droplets can be studied. Sirignano [1,4] classified interactive droplet studies into three categories: droplet arrays, droplet groups, and sprays. Arrays involve an experimentally or computationally manageable number of interacting droplets or a spatially periodic configuration with ambient gaseous conditions specified. There can be many droplets in a group but gaseous conditions far from the cloud are specified and are not coupled with the droplet calculations. In the array theory, location of each droplet is specified as an initial condition and tracked in time. Fluid dynamics and transport, including flame structure, is carefully tracked throughout the continuous gaseous volume

surrounding the droplets. Group theory handles more droplets but addresses the physical phenomena in the gas between and surrounding droplets in an averaged and modeled fashion without the complete resolution of array theory. Group theory does not assign specific locations and specific motions to droplets; only average droplet spacing and average velocity are addressed for an ensemble of droplets. Array theory does determine specific droplet location and velocity. The spray theory differs from the group theory in that the total gas-field calculation in the domain is strongly coupled to the droplet calculation. That is, there is no well defined ambience as distinct from a cloud of droplets.

Some further distinctions amongst arrays, groups, and sprays will be introduced. Also, the relevant and interesting history of group theory will be presented here. However, this review will focus on array theory for the study of liquid fuel vaporization and burning and the resolution of the fluid dynamics, transport, and flame structure within and around the droplet cloud, including the dynamic and thermal behavior of the liquid phase. Accordingly, a complete review of spray combustion is not presented here but such a broader review can be found elsewhere [1].

A cloud or collection of droplets occupies a certain volume. These primary ambient-gas conditions are defined as those conditions in the gas surrounding the cloud of droplets. Each droplet in the cloud has a gas film surrounding it. The local ambient conditions will be defined as the gas properties at the edge of the gas film but within the volume of the cloud. This definition becomes imprecise when the gas films of neighboring droplets overlap; one can cite that fact only as evidence of conceptual weakness in the theory. In such a case, the local ambient conditions would be replaced by some average over the gas in the droplet neighborhood.

There are several levels of interaction among neighboring vaporizing and burning droplets in a spray. If droplets are sufficiently far apart, the only impact is that neighboring droplets (through their exchanges of mass, momentum, and energy with the surrounding gas) will affect the gaseous ambient conditions surrounding any given droplet. For these spacings between droplets, the transport and aerodynamic characteristics, given by the Nusselt number, Sherwood number, and lift and drag coefficients, are practically identical in values to those for an isolated droplet. As the average distance between droplets increases, the influence of neighboring droplets becomes smaller and tends toward zero. A number of analyses have addressed the change in local conditions and its effects, without modification of droplet Nusselt number, Sherwood number, and/or drag coefficient from the values for an isolated droplet [5–15].

At the next level of greater interaction, droplets are closer to each other, on average, and the geometrical configurations of the exchanges with the surrounding gas are modified. In addition to modification of the local ambient conditions, the Nusselt number, Sherwood number, and the lift and drag coefficients are influenced and differ from the isolated-droplet values. Annamalai and Ryan [16] made an interesting review of interactions.

As droplets become closer to each other on average (i.e., increasing droplet number density), the geometry and the scale of the diffusion field surrounding each individual droplet will be affected. For example, we expect the Nusselt number and the functional form of the relationship between vaporization rates and local ambient conditions would be affected by the droplet spacing. This functional relationship is called the vaporization law. Its limiting form will be that given for isolated droplets. This effect of droplet spacing will also modify heat and mass transfer and vaporization rates. A decrease in droplet spacing leads to an increase in local ambient fuel-vapor concentration and a decrease in local ambient temperature because the distance from the flame is actually increased. The implication is that this, by itself, would tend to decrease the heat and mass transfer rates. Additionally, a decrease in the gas diffusion length scale should occur as droplet spacing decreases which, by itself, would increase rates. However, the net effect of a decrease in droplet spacing is to decrease the transfer and vaporization rates. Several researchers have examined a few droplets or spheres in a well-defined geometry or a large number of droplets in a periodic configuration. Here, the changes in Nusselt number, Sherwood number, and/or drag coefficient from the isolated-droplet values were determined [17–42].

Let us define these arrangements as droplet arrays. These arrays are artificial and contrived but can be useful in obtaining information about the nature of the droplet interactions. Droplet group theory is distinct (from array theory) in that a statistical description of droplet spacing (rather than a precise geometrical description) is used. In particular, a number density of the droplets is considered. As a practical matter, group theory can deal with many more droplets than array theory. An exception occurs when the array is geometrically periodic since then array theory can be used to analyze one cycle but in principle can give the behavior of an infinite number of droplets. Group theory and array theory are not useful in studying the effect of droplets on the primary ambient-gas conditions since those conditions are prescribed. Droplet vaporization rates will be shown to depend on distance from the nearest neighboring droplets and on the size of the droplet array; thus, a method which uses a representative droplet and then multiplies vaporization rate by the number of droplets being represented cannot accurately determine the effect of neighboring droplets.

Array theory is conducive to the analysis of the transport and aerodynamic characteristics but group theory is not. In group theory, the functional relationship between the local ambient conditions and the vaporization rate must be prescribed while in array theory it can be determined by analysis. This is a consequence of the detailed field analysis of array theory versus the averaging or statistical approach of group theory. Array theory can be used to determine the Nusselt number for a droplet in the array or to obtain the mathematical relationship between vaporization rate and local conditions; then, the result of that analysis can be postulated as an input for a group-theory analysis.

Spray vaporization theory will be understood to be distinct from the theory of droplet array vaporization or the theory of droplet group vaporization in that the full coupling among the ambient-gas properties, the local-gas properties, and the droplet properties is considered. Again, a statistical or average representation of properties is made on account of the large number of droplets considered. The effects of droplet spacing on Nusselt number and vaporization law can be included in spray theory. However, no investigator has included that phenomenon in their model. Obviously, this is a serious neglect for dense sprays, i.e., sprays for which the average distance between droplets is comparable with or less than the size of the gas film surrounding an average droplet.

In the next two sections, the earliest theories for droplet array theory and group theory, respectively, will be reviewed. In the fourth section, recent developments in array theory will be presented for situations of vaporizing and burning liquid fuel without forced or natural convection. In the fifth section, the affects of droplet motion and forced convection will be examined. A brief discussion of the possible use of the super-scalar in connection with array theory and droplet burning analysis is given in the sixth section. Finally, the seventh section will provide comments on the undeveloped area of turbulent, droplet array vaporization and burning. Results from particle-laden, turbulent flows without phase change or chemical reaction will be examined for useful insight and guidance in theory formulation.

2. Early studies on droplet array vaporization and combustion

The early studies on droplet arrays considered Stefan convection created by the stream of vapors from the vaporizing droplets; however, forced and natural convection were not considered. Two burning droplets of equal size were analyzed by Twardus and Brzustowski [17,18], who used a bispherical coordinate system to facilitate their analysis. Stefan convection and forced convection were not considered in the analysis. There is a critical value of the ratio of the distance between droplet centers to the droplet radius, above which the droplets burn with two individual and separate flames and below which the two droplets burn with one envelope flame. The critical value depends on the particular stoichiometry; for normal heptane, the value 17.067 was reported by Twardus and Brzustowski. The vaporization rate remains diffusion controlled and the rate of diffusion (and therefore the vaporization rate) decreases as the droplet spacing decreases. In the limit as the droplets make contact, the vaporization becomes a factor of log 2 (=0.693) of the value for two distant and isolated droplets.

Two important conclusions can immediately be seen. First, spacing between droplets in typical fuel sprays will be smaller than this critical value. Chigier and McCreath [2] have cited experimental evidence that droplets in combustors rarely burn in an isolated fashion; rather, a flame envelops many droplets. Also, the interaction between (or effectively the merging of) the gas films surrounding droplets leads to a reduction in heat transfer, mass transfer, and vaporization rates. In the quasi-steady, non-convective situation considered, a d^2 law for vaporization still exists but the coefficient is less than the value for an isolated droplet.

Labowsky [20] showed that Stefan convection can be easily included by means of a transformation that reduced the mathematical form to that for slow vaporization. The theory is general and allows for an arbitrary number of particles of varying initial size and initial temperature. The quasi-steady assumption is made, and thermodynamic equilibrium is assumed for the fuel vapor at the surfaces. The general conclusions are that (i) the vaporization rate is proportional to the vaporization rate for an equivalent isolated droplet times a corrective factor, (ii) the corrective factor decreases as droplet spacing decreases (obviously, it is unity for infinitely large spacing), and (iii) the droplet temperatures are independent of droplet spacing. (The last conclusion may be correct only under the assumption of unitary Lewis number since heat transfer and mass transfer have opposite effects on gas temperature.)

Labowsky [20,21] formulated an approach using mass-flux potential functions that could be used to treat vaporization and burning of well defined arrays with any number of droplets. Umemura [24] has provided an interesting review on that approach with emphasis on asymptotic methods. Labowsky's approach has been generalized to address vaporization with burning for a far greater number of droplets in the array [35–37], multicomponent liquids [38], and non-unitary Lewis numbers [39].

3. Early studies on droplet group vaporization and combustion

In this section, we discuss representations of vaporization of clouds for which the precise position of each droplet is not prescribed or determined and only such average quantities as droplet number density (or, equivalently, the average distance between droplets) are important. Typically, the behavior of some "average" droplet in the group or spray is discussed. This is a key aspect which distinguishes group theory from array theory. The early studies on droplet groups considered Stefan convection created by the stream of vapors from the vaporizing droplets; forced convection was not treated analytically other than through application of an empirical correction. Theories [5–7,43,44] that use continuum representations of droplets as distributed monopole sources of fuel vapor are included herein. Also included are representations (Labowsky and Rosner [44]; Samson et al. [45]) of droplets as discrete monopole sources with such a high number density of droplets that the distinction between discrete and continuum representations is not significant.

Certain distinct regimes of combustion have been discovered: isolated droplet combustion, internal group combustion, external group combustion, and sheath combustion. The particular regime of operation will be determined by droplet number density, the primary ambient conditions, droplet radius, and fuel volatility. Chemical kinetics is, of course, an important factor as well, but it is typically considered to be quite fast.

Chiu and co-workers [5–7] consider a quasi-steady vaporization and diffusion process with infinite kinetics and show the importance of a group-combustion number given by

$$G = 3\left(1 + 0.276Re^{1/2}Sc^{1/3}\right)Le\,N^{2/3}(R/s) \tag{1}$$

where Re, Sc, Le, N, R, and s are the Reynolds numbers based on diameter, Schmidt number, Lewis number, total number of droplets in the cloud, instantaneous average droplet radius, and average spacing between the centers of the droplets, respectively. This Chiu number G increases with Reynolds number, Prandtl number, and the size of the cloud (measured in droplet numbers) while it decreases with increasing Schmidt number and spacing between droplets.

The value of the Chiu number G has been shown to have a profound effect on the flame location and distributions of temperature, fuel vapor, and oxygen. Four types of behavior are found: for large G numbers, external sheath combustion occurs; then, as G is progressively decreased, external group combustion, internal group combustion, and isolated droplet combustion occurs. These regimes are identified in Fig. 1. Isolated droplet combustion involves a separate flame enveloping each droplet. Typically a group

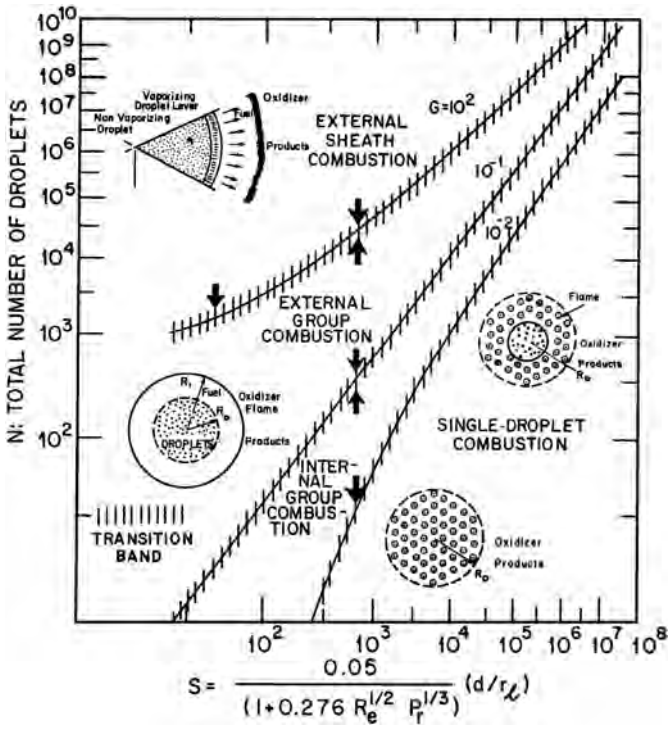

Fig. 1. Effect of group number on type of spray combustion [7].

number of less than 10^{-2} is required. Internal group combustion involves a core within the cloud where vaporization is occurring with the core totally surrounded by a flame. Outside of the core, each droplet is enveloped by individual flames. This occurs for G values above 10^{-2} and somewhere below unity. As G increases, the size of the core increases. When the single flame envelops all droplets, we have external group combustion. This phenomenon begins with G values close to the order of unity so that many industrial burners and most gas-turbine combustors will be in this range. With external group combustion, the vaporization rate of individual droplets increases with distance from the center of the core. At very high G values (above 10^2) only the droplets in a thin layer at the edge of the cloud are vaporizing. This regime has been called external sheath combustion by Chiu and co-workers.

Labowsky and Rosner [44] have found similar results. They use a quasi-steady continuum approach similar to that of Chiu and co-workers and also use a superposition method with discrete monopole sources. Labowsky and Rosner also show that the Thiele modulus $(3\phi)^{1/2}R_c/R$ is an important parameter in the determination of the onset of internal group combustion. Here, ϕ is the volume fraction of droplets and R_c is the radius of a spherical cloud of droplets. The square of that factor, $(3\phi)R_c^2/R^2$, is a Damköhler number, as stated by the authors. This Damköhler number can be readily shown to be equal to $3N^{2/3}R/S$ so that it equals the group-combustion number of Chiu and co-workers for the case of zero Reynolds number and unitary Lewis number.

Correa and Sichel [43] perform an asymptotic analysis for large G values and obtain external sheath-combustion results that agree well with those of Chiu and co-workers. A d^2 law based on cloud size is obtained in this quasi-steady sheath limit. They do raise concerns about whether the quasi-steady formulation will apply for lower values of G.

Two major shortcomings can be cited in the existing theories. First, the theories do not account for the fact that the Nusselt number and the vaporization law for each droplet will depend on the spacing between droplets (with one exception to be mentioned below). Second, the theories are quasi-steady and do not consider transient droplet heating or unsteady gas-phase conduction across the clouds. Since the time scale for droplet heating and the time and length scales for conduction across the cloud can be large, these types of unsteadiness can be profound. So, the above theories are a base for further studies rather than complete theories.

4. Potential function theory for droplet array vaporization and burning

Imaoka and Sirignano [35–37], Sirignano and Wu [38], and Sirignano [39] have developed a theory for droplet array vaporization and burning based on the approach of Labowsky. Only Stefan convection without forced or natural convection is considered here. A mass-flux potential function is defined and is the solution to Laplace's equation in the gas field. This approach is powerful because the scalar properties in the gas surrounding the droplets in the array become uniform-valued across each surface of constant mass-flux potential. So, the three-dimensional scalar field becomes one-dimensional in terms of the potential. The normalized potential function is solved in the three-dimensional space; it depends only on the geometrical configuration of the droplets in the array and not on other parameters of the problem, giving the three-dimensional solution for the potential a more universal character.

4.1. Basic formulation

A quasi-steady gas-phase and one-step chemical reaction are required. Fourier heat conduction and Fickian mass diffusion apply. All liquids have identical single-component compositions. Radiation is neglected. Phase equilibrium exists at the liquid surfaces, and the gas is negligibly soluble in the liquid. Kinetic energy, viscous dissipation, and other terms of the order of the square of the Mach number will be neglected. The momentum equation subject to these assumptions yields that the pressure is of the order of the square of the Mach number and, in the calculation of the scalar properties, it can be considered as constant. The steady-state continuity equation, energy conservation, and species conservation equations apply.

$$\nabla\cdot\left(\rho\vec{V}\right) = 0 \tag{2}$$

$$\nabla\cdot\left(\rho\vec{V}h - \lambda\nabla T - \sum_{m=1}^{N}\rho D_m h_m \nabla Y_m\right) = -\dot{\omega}_F Q \tag{3}$$

$$\nabla\cdot\left(\rho\vec{V}Y_m - \rho D_m\nabla Y_m\right) = \dot{\omega}_m \quad m = 1,\ldots,N \tag{4}$$

Sensible mixture enthalpy h, species enthalpy h_m, specific heat c_p, and mixture thermal conductivity λ are computed with the following.

$$h = \int_{T_{ref}}^{T} c_p(T')\mathrm{d}T'; h_m = \int_{T_{ref}}^{T} c_{p,m}(T')\mathrm{d}T'; c_p = \sum_m c_{p,m}(T)Y_m; \quad \lambda = \sum_m \lambda_m(T)Y_m \tag{5}$$

If there is zero tangential velocity at the liquid surface, if scalar properties are uniform on the liquid surface, and if the gas flow is irrotational, the gas-phase mass flux is governed by a potential function ϕ, such that

$$\rho\vec{V} = \nabla\phi. \tag{6}$$

From Eq. (2), ϕ satisfies Laplace's equation and the following boundary conditions.

$$\nabla^2\phi = 0 \quad \begin{cases} \phi = 0 & \text{at liquid surfaces} \\ \phi = \phi_\infty & \text{far from the liquid} \end{cases} \tag{7}$$

The existence of a potential function requires an irrotational velocity field and the alignment or counter-alignment of the density gradient and velocity vectors throughout the gas-field. Velocities at the liquid–gas interface will not have a tangential component since scalar properties are uniform over the liquid surface. Species and energy balances at the liquid surfaces indicate that the quantity $L_{eff}/(1-Y_{Fs})$ is spatially uniform over all liquid surfaces. Therefore, the instantaneous liquid surface temperature T_s and the potential function ϕ will also be spatially uniform at all liquid surfaces. The equations shown here will apply to vaporization with and without combustion.

The analysis of the gas phase will be considered first. The liquid-phase heating can be represented by the models previously discussed. The phase-equilibrium interface condition can be used for single-component fuels while, for multicomponent liquids, Raoult's Law should be employed. For multicomponent liquids, the liquid-phase mass diffusion equations must also be used.

4.2. Combustion analysis

Fast chemical kinetics prevents oxygen from diffusing to the liquid surface, and a unitary Lewis number, $\rho D = \lambda/c_p$, is required. The Shvab-Zeldovich form of the species and energy conservation equations apply.

$$\nabla\cdot\left(\rho\vec{V}\alpha_i-\rho D\nabla\alpha_i\right)=0\quad i=1,2 \tag{8}$$

The coupling functions are defined as

$$\alpha_1=h+\nu QY_O,\quad \alpha_2=Y_F-\nu Y_O. \tag{9}$$

A solution can be found whereby the advection and diffusion of the scalar coupling function variables (9) are aligned (or counter-aligned) with each other and with the Stefan flow streamlines. Using A_i as a constant to be determined, one obtains

$$\rho\vec{V}\alpha_i-\rho D\nabla\alpha_i=A_i\rho\vec{V}\quad i=1,2 \tag{10}$$

Substitution of (6) into (10), rearrangement, integration along any path, and setting $\phi=0$ at the liquid surfaces yields

$$\frac{\alpha_i-A_i}{\alpha_{i,S}-A_i}=e^{\int_0^{\phi}\frac{d\phi'}{\rho D}}\quad i=1,2 \tag{11}$$

Evaluation of Eq. (11) in the far-field yields the relation for ϕ_∞.

$$\phi_\infty=\widehat{\rho D}\ln\left(\frac{\alpha_{i,\infty}-A_i}{\alpha_{i,S}-A_i}\right)=\widehat{\rho D}\ln(1+B)\quad i=1,2 \tag{12}$$

The definitions are made that

$$\widehat{\rho D}=\frac{\phi_\infty}{\int_0^{\phi_\infty}\frac{d\phi'}{\rho D}}, \tag{13}$$

$$B=\frac{h_\infty-h_s+\nu QY_{O\infty}}{L_{eff}}=\frac{\nu Y_{O\infty}+Y_{Fs}}{1-Y_{Fs}}, \tag{14}$$

In this case, both Spalding transfer numbers are identical, i.e., $B_M=B_H$ and are denoted simply as B.

Energy balance at the interface yields the constant A. At the droplet–gas interface, $\nabla T=(\nabla h)/c_p$ and since no oxygen reached the vicinity of the interface, we find

$$\nabla\ln\left(h-h_s+L_{eff}\right)=\frac{\nabla\phi}{\lambda/c_p}, \tag{15}$$

and

$$L_{eff}=L+\frac{\dot{q}_l}{\left|\rho\vec{V}\right|_s}. \tag{16}$$

The term $\dot{q}_l$ is the magnitude of the conductive heat flux into the liquid when droplets are not at wet-bulb temperatures. There is an arbitrariness of a constant in the determination of ϕ; taking $\phi_S=0$ implies that the same thermodynamic conditions exist at all interfaces.

Since $Le=1$ implies that $\rho D=\lambda/c_p$, these values will be used interchangeably wherever necessary. Eqs. (11) and (12) are combined to yield

$$\frac{\alpha_i-A_i}{\alpha_{i,S}-A_i}=(1+B)^{\int_0^{\Phi}\frac{d\Phi'}{\lambda/c_p}}. \tag{17}$$

Application of boundary conditions provides the values of A_i. Then, from Eqs. (9) and (17),

$$(1+B)^{\widehat{\rho D}\int_0^{\Phi}\frac{d\Phi'}{\lambda/c_p}}=1+\frac{h-h_s+\nu QY_O}{L_{eff}}=1+\frac{Y_F-Y_{Fs}-\nu Y_O}{Y_{Fs}-1}. \tag{18}$$

The definition is made that

$$\widehat{\lambda/c_{p,F}}=\frac{\phi_\infty}{\int_0^{\phi_\infty}\frac{d\phi'}{\lambda/c_{p,F}}}=\left(\int_0^1\frac{d\Phi'}{\lambda/c_{p,F}}\right)^{-1}. \tag{19}$$

where a normalized potential function Φ is defined such that $\Phi=\phi/\phi_\infty$. The normalized potential function in any geometry satisfies Laplace's equation with the following boundary conditions.

$$\nabla^2\Phi=0\quad\begin{cases}\Phi=0 & \text{at liquid surfaces}\\ \Phi=1 & \text{far from the liquid}\end{cases} \tag{20}$$

For a given geometrical description of the liquid surfaces, Φ can be determined. There is no explicit dependence on liquid-fuel choice, transport properties, and scalar boundary values; these parameters only appear through the normalization factor. Implicitly, the act that Φ has the same value at every point on a gas–liquid interface means that surface temperature and fuel–-vapor mass-fraction surface values are uniform. They may however vary with time. Of course, situations with non-uniform surface values can be expected; so, caution is needed in interpretation of results.

Although the Φ value is identical at all points on a droplet surface, the gradient of Φ at the surface is always normal to the surface but its magnitude can vary along the surface. This situation implies that heat and mass flux can vary along the surface. The solution of the Laplace equation is coupled with the solution of an unsteady heat diffusion equation for each droplet. The heat equation has been solved assuming spherical symmetry and using boundary fluxes averaged over a droplet surface. Even though droplets have the same surface temperature, heating rates and vaporization rates will vary depending on the droplet location in the array [37].

Y_{Fs} can be obtained as a function of surface temperature at atmospheric pressure using a phase-equilibrium relation such as the Clausius–Clapeyron relation, which is independent of configuration and ambient conditions other than pressure. The mass fraction of fuel vapor at the interface increases substantially with time as the droplet heats. This will have a dramatic effect on the temporal behavior of the vaporization rate. For any configuration, the vaporization rate can be shown to be directly proportional to $\ln(1+B)$ which by itself is independent of configuration (i.e., droplet radius and spacing) or transport properties. The quantity L_{eff} is a measure of the energy conducted from the gas to the liquid surface per unit mass of vaporized fuel. The product of L_{eff}/L and $\ln(1+B)$, which we define as w, is a critical factor in the evaluation of the normalized energy per unit time conducted to the liquid surface. w, which is independent of configuration but dependent on Lewis number, would be multiplied by factors dependent on transport properties and configuration to obtain the actual rate.

Noting that $Le=1$, the combination of Eqs. (12) and (13) yields the following relation.

$$\widehat{\rho D}=\widehat{\lambda/c_p}=\left(\int_0^1\frac{d\Phi'}{\lambda/c_p}\right)^{-1} \tag{21}$$

In the limit of infinite-rate chemical kinetics, the flame surface will lie on the constant Φ surface denoted by Φ_F. This value is determined implicitly via the following expression.

$$\frac{\ln(1-Y_{Fs})}{\ln(1+B)} = -\widehat{\rho D}\int_0^{\Phi_F}\frac{d\Phi'}{\lambda/c_p} \tag{22}$$

The system of Eqs. (18)–(22) yield the four relations necessary to determine the values of $\widehat{\rho D}$, the flame contour Φ_F, mixture enthalpy h, and fuel vapor mass fraction Y_F. Fuel type, T_∞, $Y_{O\infty}$, and T_s are treated as parameters in the calculations. Eqs. (18) and (21) are coupled because transport properties and specific heat depend on temperature and composition. When the liquid surface temperature is less than the wet-bulb value, phase equilibrium dictates that B be calculated with the last term in Eq. (14). The first term then provides the liquid heating rate through L_{eff}. With the assumption $\rho D = \lambda/c_p = \overline{\rho D}$ = constant, Eqs. (18)–(22) are simplified and uncoupled. Then,

$$(1+B)^{\Phi} = 1+\frac{h-h_s+\nu QY_O}{L_{eff}} = 1+\frac{Y_F-Y_{Fs}-\nu Y_O}{Y_{Fs}-1}, \tag{23}$$

$$\Phi_F = \frac{-\ln(1-Y_{Fs})}{\ln(1+B)}. \tag{24}$$

Eqs. (23) and (24) would still result if the constant value of $\rho D = \lambda/c_p$ were defined arbitrarily, without accordance to Eq. (21): for example, if the value is taken at infinity or at the liquid surface.

In either the variable ρD or constant ρD situation, the vaporization rate of the jth droplet (or any portion of the liquid surface designated as the jth segment) is obtained by integrating the mass flux over the droplet (segment) surface.

$$\dot{m}_j = \iint \nabla\phi\cdot d\vec{A}_j = \widehat{\rho D}\ln(1+B)\iint \nabla\Phi\cdot d\vec{A}_j \tag{25}$$

It is not uncommon for droplet vaporization rates to be normalized by the vaporization rate of an isolated droplet at the wet-bulb temperature. In the literature, this has often been referred to as a burning rate correction factor or an interaction coefficient, η. Then, for the jth droplet,

$$\eta_j = \frac{\dot{m}_j}{\dot{m}_{iso}} = \frac{1}{4\pi R_j}\iint \nabla\Phi\cdot d\vec{A}_j. \tag{26}$$

The vaporization rate of an isolated droplet at wet-bulb temperature with variable $\rho D = \lambda/c_p$ is given by

$$\dot{m}_{iso} = 4\pi\left(\int_R^\infty \frac{dr}{(\lambda/c_p)r^2}\right)^{-1}\ln(1+B). \tag{27}$$

For a single, isolated droplet, the solution to Eq. (20) yields $\Phi_{iso} = 1 - R/r$. Upon substitution with (21), Eq. (27) can be expressed as

$$\dot{m}_{iso} = 4\pi R\widehat{\rho D}\ln(1+B). \tag{28}$$

Therefore, within this generalized analysis, a single, isolated droplet is a special case for which the solution Φ to Eq. (20) can be obtained analytically. The above formulas for vaporization rate are the same with and without an envelope flame. The value of the transfer number B would differ in those two cases.

The use of normalized vaporization rates as in Eq. (26) has been the standard for authors studying multiple droplet arrays. Although this practice does provide an assessment of the effect of droplet interactions, several key aspects are obscured. To obtain an actual (dimensional) vaporization rate, one would refer to Eq. (26) with η known for a specific geometry. However, the vaporization rate of an isolated droplet, and more specifically the value of $\rho D = \lambda/c_p$, is not obvious. In many works, ρD is assumed constant, yet in practice it will vary spatially in the gas-phase. No mention of the appropriate value, or an appropriate average value has been presented prior to the studies of Imaoka and Sirignano. This is possibly due to the absence of liquid-heating, where the numerical value of $\rho D = \lambda/c_p$ would have been required. Law [46], and Law and Sirignano [47] include liquid-phase heating for an isolated drop but use a constant value for ρD.

The results for η_j are independent of the choice of the reference length. This means that η_j will depend only on length ratios, e.g., droplet-diameter-to-droplet-spacing ratio, and not on actual size. So, if all lengths are scaled upwards or downwards in proportion, η_j will not change in value. The average nondimensional vaporization rate for a droplet array of N droplets can be found as $\eta_A = (\sum_{j=1}^{N}\eta_j)/N$.

In these nondimensional forms, the vaporization rates η_j and η_A are independent of liquid-fuel choice, transport properties, and scalar boundary conditions. They depend only on geometrical configuration so that previous computational results can be employed. In particular, the computational correlation $\eta(\xi)$ of Imaoka and Sirignano [35,37] can be used. That is

$$\eta_A = 1-\frac{1}{1+0.725671\xi^{0.971716}}$$
$$\xi = \frac{\left[\frac{4\pi V_A N}{3V_l}\right]^{1/3}}{[N^{1/3}-1]N^{0.72}} \tag{29}$$

where V_A,V_l, and N are the array volume, total liquid volume, and droplet number, respectively. So, if only vaporization rates are desired, it is not necessary to obtain the field solution for various array configurations by solving Laplace's equation. Note that, after the volume ratio in Eq. (29) is related to the ratio of droplet spacing to droplet radius, the reciprocal of ξ can be shown to be a constant times the Chiu number in the limit of very large N and zero Reynolds number. However, while Chiu's theory produces a similar dimensionless group, it does not account for changes in Nusselt number or Sherwood number due to the proximity of other droplets.

Note that Eq. (29) and much of the previous formulation apply only if every droplet has the same instantaneous surface temperature. That assumption will not hold during transient heating of a large, closely-packed array where the inner droplets are given heat protection by the outer droplets.

Eq. (29) presents very useful information. For example, it shows that, if total liquid volume and array volume remain fixed and droplet number is large compared to one, vaporization rate and burning rate decrease as the number of droplets increase with consequential decrease in initial droplet size.

The analysis applies universally to all droplet array sizes and geometries. As previously mentioned, other liquid–gas interface problems are also included. Geometrical effects are calculated separately through the potential function Φ, and are independent of gas-phase transport properties and boundary conditions. Consequently, the problem for the scalar properties is one-dimensional for any configuration while the three-dimensional analysis is necessary only in solving Eq. (20).

The scalar quantities T, Y_F, and Y_O are shown versus Φ in Fig. 2 for decane fuel, with T_∞ = 298 K and $Y_{O\infty}$ = 0.231. The ambient pressure is 1 atm in all of the calculations. A large variation in flame location for decane compared to lower-molecular-weight fuels is caused by the larger wet-bulb temperature and lower volatility resulting in lower values of Y_{FS} at 298 K than for the other fuels. An increase in ambient oxidizer mass fraction leads to higher flame temperatures and brings the flame closer to the liquid surface as

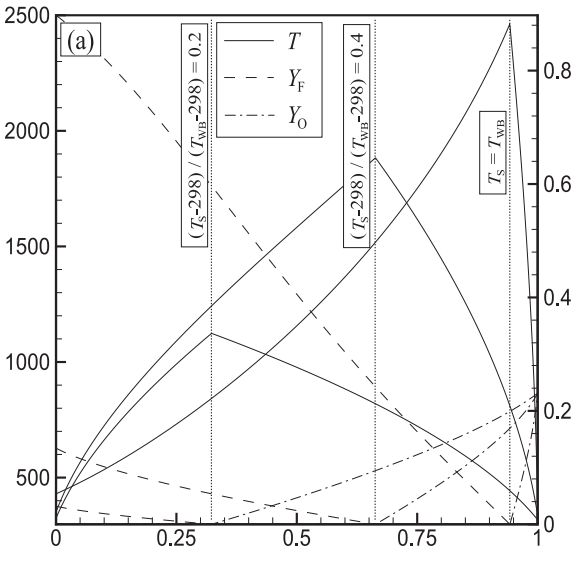

Fig. 2. Temperature, fuel and oxidizer mass fractions versus Φ with $T_\infty = 298$ and $Y_{O\infty} = 0.231$ for various surface temperatures for decane, $T_{WB} = 429.73$ K [36].

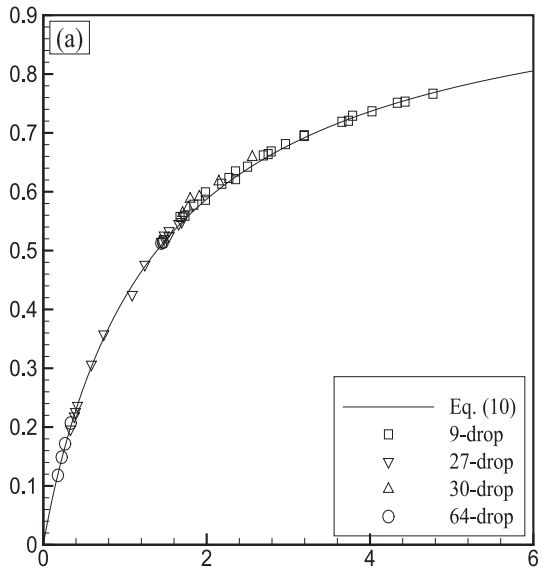

Fig. 3. Normalized array vaporization rates for various arrays with non-uniform spacing versus the similarity parameter ξ [37]. Eq. (10) in the reference is identical to Eq. (29) here.

expected. The proximity of the flame to the liquid surface for a low volatility fuel introduces the possibility of individual droplet flames for low droplet surface temperatures. However, the occurrence of individual flames will depend strongly on the array geometry.

Gas-phase scalar variables, transport properties, specific heats, and flame locations for a specified fuel type and boundary conditions depend only on the potential function and liquid surface temperature. Therefore, the problem for the scalar properties becomes one-dimensional for any configuration while the three-dimensional analysis is limited to the solution of Laplace's equation. Flame stand-off distances are found to decrease by more than a factor of two when the quantity ρD is not assumed constant.

Imaoka and Sirignano [35] have shown that, in a 125-drop mono-sized cubic array with $d/a = 3$, the outermost droplet will vaporize more than 5000 times faster than the central droplet of the array. However, the induced Stefan velocity leaving the array might further enhance the burning rates of the outer droplets, making the factor of 5000 a conservative estimate. At that same spacing but with 1000 droplets, the difference is more than a factor of 10^7. Since the current problem formulation permits only normal velocities at the droplet surfaces, the effects of very strong blowing velocities from the inner droplets creating boundary layers over the outer droplets are not included in the analysis.

Consider now an array with non-uniform droplet spacing. The average spacing is calculated on a volumetric basis: $d = V_A^{1/3}/(N^{1/3} - 1)$ where V_A is the array volume of a polyhedron surface drawn using the centers of the outermost droplets. The level of agreement between the vaporization data yielded through solution of Laplace's Equation and the curve fit for uniform droplet spacing given by Eq. (29) is shown in Fig. 3. The curve-fit is also excellent for cases with non-uniform initial droplet radii as indicted by Fig. 4. Vaporization rates for arrays consisting of droplets in a line or in a plane are not predicted well because spacing is infinite in one direction. For a finite number of droplets with infinite droplet spacing, the total vaporization rate of the array will be $4\pi\widehat{\rho D}\ln(1+B)$ multiplied by the sum of the droplet radii.

The calculations [35] show that different types of flames structures can arise depending on normalized droplet spacing and droplet surface temperature. So, the structure can evolve as droplets heat and as droplet radii decrease with time due to vaporization, causing an increase in the normalized droplet spacing. For low temperature and large normalized spacing each droplet can be surrounded by its individual flame. As surface temperature increases or normalized spacing spacing decreases, the innermost droplets in an array will share a common flame envelop while outer droplets have individual flames. With continued change in the indicated directions, all droplets in the array can have one group flame. Under all situations, the outer droplets will vaporize faster than inner droplets. During the lifetime of an array, it is possible to start with individual flames due to lower surface temperature values. The droplets will initially heat faster than they vaporize; so, a group flame would tend to form. As the surface temperature approaches the wet-bulb temperature, vaporization will become faster decreasing droplet size without substantial change in surface temperature. So, a return to individual flames can occur.

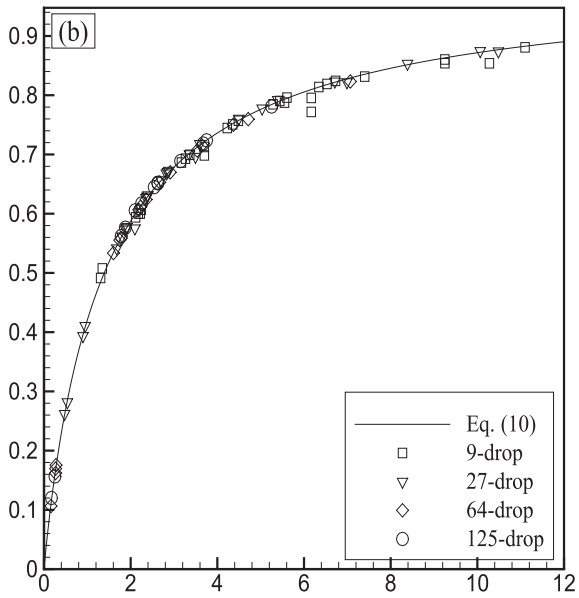

Fig. 4. Normalized array vaporization rates versus the similarity parameter ξ for variations in droplet radii [37]. Eq. (10) in the reference is identical to Eq. (29) here.

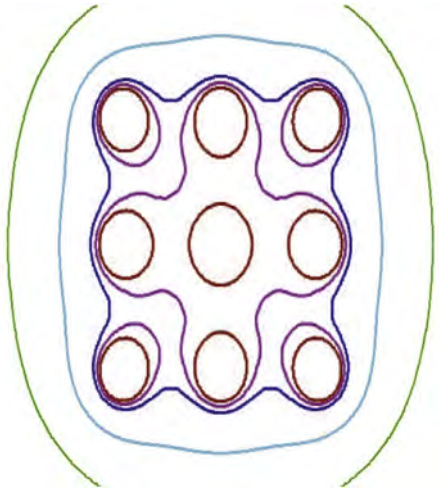

Fig. 5. Outer plane flame shapes for 27 droplets in a cubic array. The five contours give flame positions at different droplet surface five temperatures: 285, 295, 305, 315, and 325 K. The flame moves farther from the droplet surface with increasing surface temperature [35].

Figs. 5 and 6 show results at different surface temperature values for a cubic array with 27 droplets (i.e., $3 \times 3 \times 3$). We may deconstruct the array into two outer planes with nine droplets each (i.e., 3×3) and a central plane, again with nine droplets. The figures show instantaneous flame contours at five droplet surface temperatures: 285, 295, 305, 315, and 325 K. Of course, the flame position moves farther from the droplet as the surface temperature value is raised. So, the two figures show that at 285 K, all droplets gave individual flames. At 295 K, a single group flame engulfs five droplets in the central plane and one in each outer plane, leaving twenty individual droplet flames on the outside of the group flame. At 305 K, only the eight droplets at the corners of the array have individual flames with a group flame surrounding the other nineteen droplets. Above about 310 K, only one group flame exists.

Fig. 7 shows how the radius of droplets in a symmetric array of nine droplets would decrease with time. Eight droplets are at the corners of a cube with one in the center. It is assumed that the surface temperature remains constant at the wet-bulb temperature. It is clear that deviation from the classical d^2 law becomes substantial as spacing between droplets decreases. Realize that

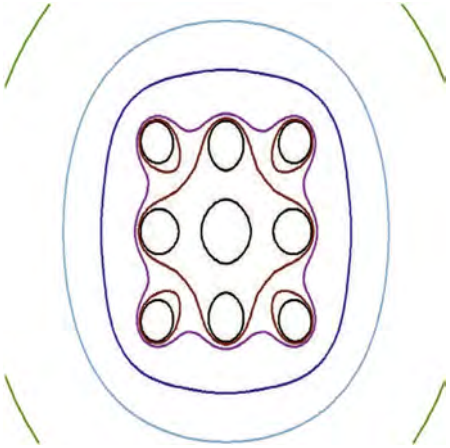

Fig. 6. Inner plane flame shapes for 27 droplets in a cubic array. The five contours give flame positions at different droplet surface five temperatures: 285, 295, 305, 315, and 325 K. The flame moves farther from the droplet surface with increasing surface temperature [35].

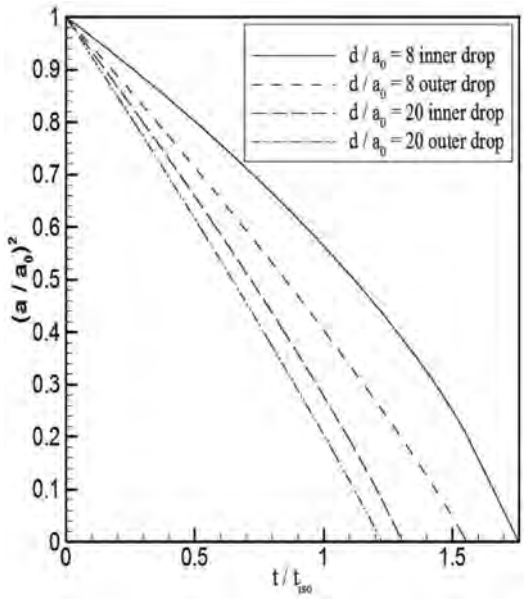

Fig. 7. Deviation from d^2 law due to neighboring droplets [37].

additional deviations will be caused by the transient heating and convective effects not present in this model. In spite of the mounting evidence, many researchers cling to the d^2 law which has outlived its usefulness for practical combustors. Further evidence of substantial deviation from a d^2 law is given in Fig. 8 where both effects of transient droplet heating and droplet spacing are portrayed. It is seen again there that as spacing decreases and thereby influence of neighboring droplets increases, the deviation from classical isolated-droplet behavior increases. Furthermore, the deviation also becomes greater as the realism of the liquid heating model improves. Greater deviation occurs with transient heating and the conduction limit model provides more deviation in droplet lifetime value than the uniform-liquid-temperature model also known as the infinite-conductivity model.

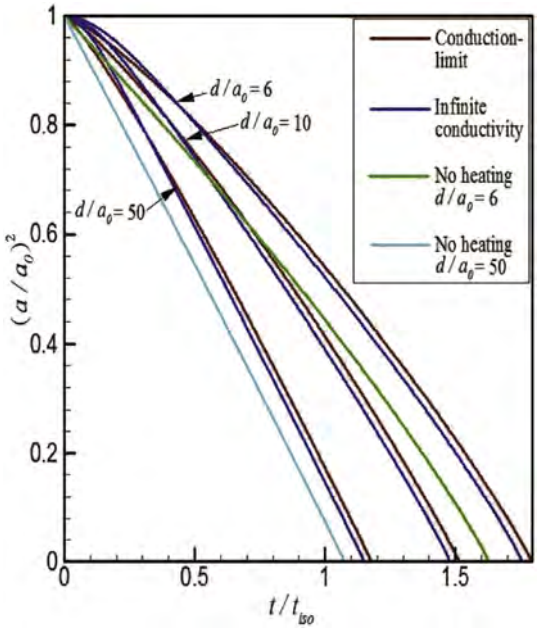

Fig. 8. Deviation from d^2 law due to liquid-phase heating [37].

Sirignano and Wu [38] extended the theory to the vaporization of multicomponent liquid droplets. Changes of liquid temperature and mass fractions for three components of varying volatility were compared for the interactive droplet case with the results of the isolated droplet case. The surface temperature rises more sharply in time at first and then more gently later. The mass fraction of the most volatile component, heptane, decreases at first then approaches a constant value at the surface. The isolated droplet has greater rates of temporal change of surface values and vaporizes faster.

During the transient behavior, there is heat conduction and species diffusion inside the droplets. Fig. 9 shows the profiles of interior temperature and heptane mass fraction at different times in the droplet lifetime. These profiles change with time while the changes of surface temperature and surface composition become slower with time. As liquid-phase heat conduction is much faster than liquid-phase mass diffusion, the temperature becomes nearly uniform and constant after some time while the species mass fraction still vary over the droplet interior. Lower ambient temperature always leads to more uniform profiles because it results in a longer lifetime and allows more time for heat and species diffusion in the droplets. For 350 K ambient temperature, the temperature profiles are nearly uniform throughout the lifetime but the mass fraction profiles are not; so, the slow vaporization limit is not strictly satisfied even at low ambient temperature 350 K. For 2000 K ambient temperature as shown in Fig. 9, the temperature and mass fraction profiles become steeper but still don't produce a sufficiently thin diffusion layer to satisfy strictly the fast vaporization limiting conditions.

Experiments on droplet arrays have been performed. Microgravity facilities have been used which eliminates buoyancy currents and allows large droplets to be examined. Kobayashi et al. [48] studied flame spread over a linear array of n-decane droplets. Mikami et al. [49] also examined flame spread along a linear array using a new technique for generating droplets. These linear-array experiments have addressed the unsteady ignition and flame spread problem whereas existing theory has addressed the quasi-steady vaporization burning. So, comparisons cannot be made. However, a clear dependence on droplet spacing is found; maximum spread rate occurs at some specific spacing and above another spacing value, spread cannot occur.

4.3. Summary of potential theory for burning fuel-droplet arrays

Array theory offers the opportunity to determine fuel-droplet vaporization and burning rates in situations where neighboring droplets will modify Nusselt number, Sherwood number, and rates of vaporization and heat release. The theory is a candidate for use in models that predict droplet rates in a dense spray where the droplet size and spacing between neighboring droplets is below the scale for numerical resolution; i.e., it forms a basis for sub-grid modeling.

In situations where forced and natural convection are not important and gas motion relative to droplets is caused mainly by Stefan convection, the use of mass flux potential is promising. Computations are reduced to the solution of Laplace's equation in the gas which is relatively simple even for complex configurations. Furthermore, the scalars in the gas phase can become "one-dimensional" functions of the potential only, without explicit dependence on time. Of course, as boundary conditions change in time, the potential and scalar fields will vary. The unsteady heat equation with account for the regressing droplet interface is all that is needed for the single-component liquid phase. For multicomponent liquids, the unsteady, liquid-phase, mass-diffusion equations must be simultaneously solved.

The results show that the dense spray environment causes substantial deviation of the droplet behavior from the isolated-droplet predictions even if we neglect the other causes for serious deviations: transient liquid heating and forced or natural convection. So, for practical situations related to combustion of liquid fuels, the d^2 law should not be used.

Peripheral droplets in the array vaporize faster than inner droplets. Droplet lifetimes are increased as the array becomes more dense. Arrays of different droplet size, droplet spacing, and total number of droplets can be characterized using a single similarity parameter. Of course, that characteristic offers a huge advantage for sub-grid modeling. Different modes of combustion can occur depending on fuel choice; ambient conditions; and droplet temperature, size, spacing, and total number. That is, individual flames for each droplet can occur; an envelope flame (group flame) surrounding inner droplets with individual flames for peripheral droplets is possible; or one group flame for all droplets is another mode. During the lifetime of the droplets, the mode can change more than once.

The utility of the conserved scalars relies on the use of one-step oxidation kinetics, low Mach number, Fourier heat conduction, and Fickian mass diffusion. Extension to non-unitary Lewis number has been made. The mass-flux potential theory is currently limited to cases where all droplets have the same temperature at any instant of time. That is a convenient assumption but not an inherent limitation. The theory should be extendable to cases where different surface temperature and, thereby, different potential values exist

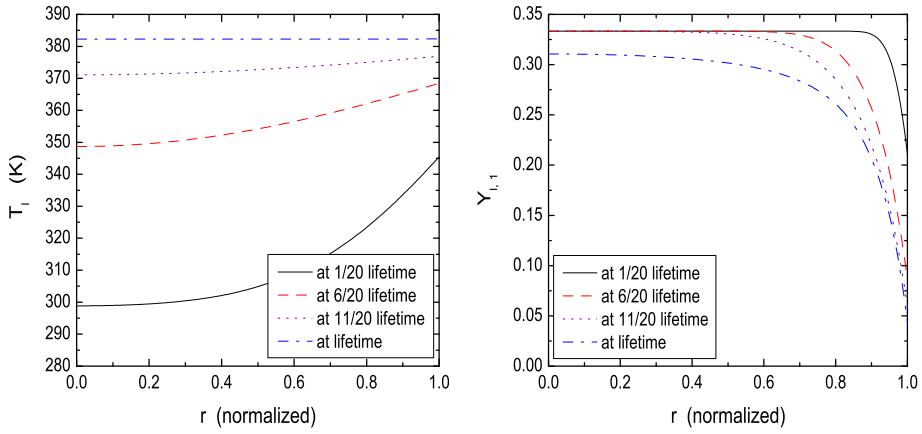

Fig. 9. Profiles of temperature and heptane mass fraction in the liquid phase during the transient behavior, with identical initial mass fraction for heptane, octane and decane. $T_\infty = 2000$ K [38].

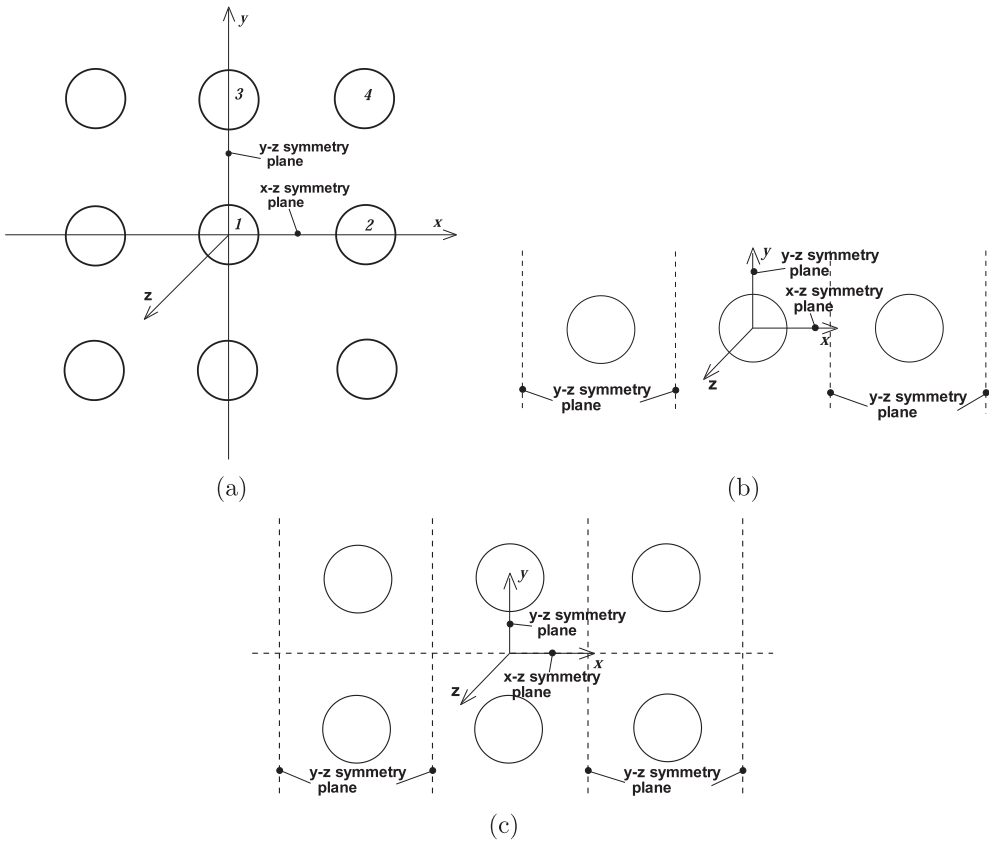

Fig. 10. The flow direction is perpendicular to the x–y plane in which the droplet centers are located. (a) The finite array with nine droplets with centers in the x–y plane and flow in the z direction (1: droplet at the plane center, 2 or 3: droplet at the edge center, 4: droplet at the corner); (b) The semi-infinite periodic array with one row of droplets, with centers in the x–y plane and flow in the z direction; (c) The semi-infinite periodic array with two rows of droplets, with centers in the x–y plane and flow in the z direction [41].

simultaneously on the surfaces of different droplets. The neglect of forced or natural convection and the quasi-steady gas-phase assumption are essential to the reduction to Laplace's equation. So, other approaches are needed to develop array theory for convective situations. That will be discussed in the next section. Also, different approaches with unsteady gas phase behavior are required for near-critical and transcritical behavior Array theory at these high pressure conditions has not been developed although isolated-droplet theory at these conditions has undergone some development [1].

5. Convective array vaporization and burning

An accurate numerical simulation should include as many features of real physics (such as forced convection) as possible under currently available computing resources. Some studies have been made in the literature on the convective vaporization of axisymmetric droplets analytically [50] and computationally [29,51] with assumption of constant thermo-physical properties. Other studies considered variable properties in the numerical simulation by Chiang et al. [30,31,52], with the conclusion that the thermal dependence of physical properties must be considered for high-temperature calculation. Convective burning of axisymmetric droplets have also been studied experimentally [53] and computationally [54–59]. Dwyer et al. [55,56] and Wu and Sirignano [57] studied the effects of surface tension and found that the surface tension had significant influence on the liquid motion inside the burning droplet. Wu and Sirignano [57] and Pope et al. [59] identified some of the transient behaviors of an isolated convecting burning droplet, with considerations of droplet regression, deceleration due to the drag of the droplet, internal circulation inside the droplet, and variable properties.

The numerical calculations for 3-dimensional configurations have been made for non-vaporizing spheres by Kim, Elghobashi and Sirignano [32], and for vaporizing and burning interactive droplets by Stapf, Dwyer and Maly [33,34] without the consideration of internal circulation in the liquid phase. They found that the interactions inside the droplet arrays had a strong influence on the flow field and the physical–chemical processes. Wu and Sirignano [40] numerically studied the transient convective burning of fuel droplets interacting within an infinite periodic array with considerations of internal circulation inside the droplets and non-uniform surface temperature. The spacing amongst droplets was found to influence the burning rate by affecting the droplet surface temperature and interactions amongst droplets.

Sirignano and Wu [40–42] simulated convecting, burning and interactive droplets in several single-layer arrays, by solving the Navier–Stokes, energy and species equations. Droplet regression, deceleration of the stream flow due to the drag of the droplets, internal circulation, variable properties, non-uniform surface temperature, and surface tension are considered. In addition to infinite, periodic single-layer array, other calculated single-layer, array configurations are shown in Fig. 10 and include semi-infinite periodic arrays, with one row or two rows of droplets, and finite arrays with nine droplets with centers in a plane. The transient flame shape, surface temperature, burning rate, and dimensionless numbers were studied for different initial droplet spacing, initial Reynolds number and initial Damköhler number. Particularly, the critical parameters for the determination of the initial flame shapes, the flame transition (from a wake flame to an

envelope flame) time and its influence on the burning rate are determined. The model arrays are qualitatively characteristic of real spray situations in which there is a very large number of droplets interacting in arrays. These models do allow substantial savings of computational resources. A real spray is of course not a single-layer array along the flow direction. However, the behavior of the single-layer array is similar to behavior of the most upstream droplets in a real spray. The various array configurations considered in this study account for some possible situations in real spray systems: the infinite periodic arrays are close to the situation when the spray is well formed and uniformly distributed, and the semi-infinite periodic arrays and finite arrays represent other situations when all or some of the droplets are less interactive than a droplet in the infinite periodic arrays. Although the results for droplets in single-layer arrays are most relevant for the most upstream droplets in a real spray, the important issues such as interactions amongst droplets, the flame configurations, and their influence on the burning rate as addressed in this study also provide some useful insight for the understanding of the fundamental aspects of a whole real spray.

5.1. Problem formulation

The infinite periodic array can be considered as a periodic array with infinite number of rows of droplets. Thereby, it is periodic in two directions. The finite array with nine droplets with centers in a plane is shown in Fig. 10(a). The semi-infinite periodic arrays with one row or two rows of droplets have infinite number of droplets only in one direction, as shown in Fig. 10(b,c). For an infinite periodic array, the 3-dimensional flows are periodic along the two directions in the plane, and thus only one droplet can be considered in the calculation using four symmetry planes. In fact, the actual domain for the calculation can be further reduced with only a quarter of the droplet due to symmetries. Similarly, the reduced number of droplets by symmetries is a quarter for semi-infinite periodic arrays with one row of droplets, a half for semi-infinite periodic arrays with two rows of droplets, and, it becomes one full droplet, two half droplets, and a quarter droplet for finite arrays with nine droplets with centers in a plane.

The free-stream air flow has velocity U_∞, pressure p_∞, and temperature T_∞. The initial droplet temperature $T_{s,0}$ is uniform and low compared to the boiling point. The droplets are first heated and vaporized, and then auto-ignited by the hot free stream and burned. Internal circulation is caused by the shear stress at the gas-side droplet surface and the non-uniform distribution of surface tension around the droplet surface. Although the droplets have a time-varying velocity U_d, we consider that they are stationary by instantaneously having an inertial frame of reference moving at the droplet velocity. The relative velocity becomes: $U'_\infty = U_\infty - U_d$. This is justified for an infinite periodic array and a semi-infinite periodic array with one row of droplets with no relative motion amongst the droplets, and for a semi-infinite periodic array with two rows of droplets with no relative motion between droplets in the flow direction and also negligible relative motion in the other two directions because of small side forces. However, for a finite array with nine droplets with centers in a plane, not all the droplets are subject to the same drag and have the same velocity, but we still assume that the relative motion amongst the droplets can be neglected and U_d is the same for all the droplets for simplicity. As the droplets are slowed by the drag and vaporization occurs, the relative velocity and droplet radius are updated continuously.

The following assumptions are made: (1) the Mach number is much less than unity and the dissipation terms are neglected; (2) there is no natural convection and other gravity effects; (3) the droplets remain spherical; (4) the gas mixture is an ideal gas; (5) the liquid-phase properties variation is neglected; and (6) the radiation is neglected.

The variables have been non-dimensionalized and are listed as follows: radial position $\bar{r} = r/d_0$, time $\bar{t} = (tU'_{\infty,0})/d_0$, velocity vector or components $\bar{u} = u/U'_{\infty,0}$, pressure $\bar{p} = p/\rho_\infty U'^2_{\infty,0}$, density $\bar{\rho} = \rho/\rho_\infty$, enthalpy $\bar{h} = h/c_{p_\infty}(T_\infty - T_{s,0})$, temperature $\bar{T} = (T - T_{s,0})/(T_\infty - T_{s,0})$, molecular weight $\overline{M_i} = M_i/M_F$, specific heat $\overline{c_p} = c_p/c_{p_\infty}$, kinetic viscosity $\bar{\mu} = \mu/\mu_\infty$, thermal conductivity $\bar{\lambda} = \lambda/\lambda_\infty$, thermal diffusivity $\bar{\alpha} = \alpha/\alpha_\infty$, mass diffusivity $\overline{D_i} = D_i/D_{i,\infty}$, shear stress tensor $\bar{\tau} = (\tau d_0)/(\mu_\infty U'_{\infty,0})$, reaction rate $\bar{\dot{\omega}} = \dot{\omega}/\dot{\omega}^o$, surface tension $\bar{\sigma} = \sigma/\sigma_0$, where d_0 and $U'_{\infty,0}$ denote the initial droplet diameter and the initial relative stream velocity. The superscript 'o' denotes the reference value, and the subscripts 'F', 'i', '∞' and '0' denote the fuel vapor, the ith species, the ambient value and the initial value, respectively. There are certain dimensionless numbers generated: initial Reynolds number $Re_0 = (\rho_\infty U'_{\infty,0} d_0)/\mu_\infty$, Prandtl number $Pr_\infty = \mu_\infty/\alpha_\infty$, Schmidt number $Sc_{i,\infty} = \mu_\infty/D_{i,\infty}$, reference Spalding number for heat transfer $B^o_H = (c_{p_\infty}(T_\infty - T_{s,0}))/L$, initial Weber number $We_0 = (\rho_\infty U_\infty, 0'^2 d_0)/\sigma_0$, and initial Damköhler number $Da_0 = (d_0/U'_{\infty,0})/(\rho_\infty Y^o_F/(\dot{\omega}^o M_F))$ (where Y^o_F is the reference mass fraction for the fuel vapor).

The governing equations for both gas and liquid phases are:

Continuity equation:

$$\frac{\partial \bar{\rho}}{\partial \bar{t}} + \bar{\nabla}\cdot(\bar{\rho}\,\overrightarrow{\bar{u}}) = 0. \tag{30}$$

Momentum equation:

$$\frac{\partial \bar{\rho}\,\overrightarrow{\bar{u}}}{\partial \bar{t}} + \bar{\nabla}\cdot(\bar{\rho}\,\overrightarrow{\bar{u}\,\bar{u}}) = -\bar{\nabla}\bar{p} + \frac{1}{Re_0}\bar{\nabla}\cdot\left(\overline{\mu\left(\nabla\overrightarrow{u} + \nabla\overrightarrow{u}^T\right) - \frac{2}{3}\mu(\nabla\cdot\overrightarrow{u})1}\right), \tag{31}$$

The divergence of $\overrightarrow{u}$ becomes 0 for the incompressible liquid phase.

Energy equation:

$$\frac{\partial \bar{\rho}\bar{h}}{\partial \bar{t}} + \bar{\nabla}\cdot\left(\bar{\rho}\,\overrightarrow{\bar{u}\bar{h}}\right) = \frac{1}{Re_0 Pr_\infty}\bar{\nabla}\cdot\left(\bar{\rho}\bar{\alpha}\bar{\nabla}\bar{h}\right) + S_h, \tag{32}$$

in which $S_h = \bar{\nabla}\cdot(\Sigma_{i=1}^N \bar{\rho}\overline{D_i}\bar{h}_i\bar{\nabla}Y_i)/(Re_0 Sc_{i,\infty}) - \bar{\nabla}\cdot(\bar{\rho}\bar{\alpha}\Sigma_{i=1}^N \bar{h}_i\bar{\nabla}Y_i)/(Re_0 Pr_\infty) + \frac{Q\bar{\omega}Y^o_F Da_0}{M_F c_{p_\infty}(T_\infty - T_{s,0})}$ for the gas phase, and $S_h = 0$ for the liquid phase. The reaction rate is given by $\dot{\omega} = Ae^{-\frac{E_a}{R_u T}}[\text{Fuel}]^a[\text{Oxidizer}]^b$ mol/cm^3 s, with $A = 4.6 \times 10^{11}$, $E_a = 1.255 \times 10^5$, $a = 0.25$, $b = 1.5$ for n-octane, from Westbrook and Dryer [60]. The reference value of the reaction rate $\dot{\omega}^o$ is calculated based on T_∞, ρ_∞, $Y_{O_2,\infty}$, and the stoichiometric mass fraction for the fuel vapor Y^o_F. The values of $\dot{\omega}^o$ and the initial Damköhler number Da_0 will be very sensitive to the choice of the reference temperature, and T_∞ is a good choice for high ambient temperature where autoignition becomes possible.

Gas-phase species equation:

$$\frac{\partial \bar{\rho}Y_i}{\partial \bar{t}} + \bar{\nabla}\cdot(\bar{\rho}\,\overrightarrow{\bar{u}}Y_i) = \frac{1}{Re_0 Sc_\infty}\bar{\nabla}\cdot\left(\bar{\rho}\overline{D_i}\bar{\nabla}Y_i\right) + \bar{\omega}S_i\overline{M}_i Y^o_F Da_0, \tag{33}$$

in which $\overline{M}_i$ and S_i are the normalized molecular weight, and stoichiometric number for the ith species which represents moles of this species produced (+) or consumed (−) for each mole of fuel consumed.

The droplet surface regresses during vaporization, and the droplet radius is a function of time. The forces on each droplet are represented using lift and drag coefficients (z-direction drag C_D, x-

direction lift C_{Lx}, and y-direction lift C_{Ly}). The droplets are slowed down by the drag in the transient process, and the instantaneous velocity of any of the droplets is determined by

$$\frac{d\overline{U}_d}{d\bar{t}} = -\frac{d\overline{U}'_\infty}{d\bar{t}} = \frac{3}{8}\frac{1}{\overline{\rho}_l}\frac{\overline{U}'^2_\infty}{\overline{R}}C_D. \tag{34}$$

The Spalding transfer numbers, Nusselt number, and Sherwood number are defined as:

$$B_H = \frac{c_{p,film}(T_\infty - T_{s,avg}) + \nu Y_{O\infty} q}{L_{eff}};\ B_M = \frac{Y_{Fs,avg} + \nu Y_{O\infty}}{1 - Y_{Fs,avg}};$$

$$Nu = \frac{\overline{R}}{2\pi\left(1 - \overline{T}_{s,avg} + \frac{\nu Y_{O\infty} q}{c_{p,film}(T_\infty - T_0)}\right)}\int_0^{2\pi}\int_0^{\pi}\overline{\lambda}_{g,s}\left(\frac{\partial \overline{T}_g}{\partial \overline{r}}\right)_s \sin\theta\, d\theta\, d\phi; \tag{35}$$

$$Sh = \frac{\overline{R}}{2\pi\left(Y_{F\infty} - Y_{Fs,avg}\right)}\int_0^{2\pi}\int_0^{\pi}\overline{\rho}_{g,s}\overline{D}_{g,s}\left(\frac{\partial Y_F}{\partial \overline{r}}\right)_s \sin\theta\, d\theta\, d\phi,$$

where ν is fuel-to-oxygen mass stoichiometric ratio (0.285 for n-octane), $c_{p,film} = c_{p\infty} + 2c_{ps,avg}/3$, and $L_{eff} = Q_{s,g}/\dot{m}$. The modified gas-phase Reynolds number is defined as $Re_m = (\rho_\infty U'_\infty d)/\mu_{film}$, with $\mu_{film} = \mu_\infty + (2\mu_{s,avg}/3)$.

The thermophysical properties for the gas mixture are calculated by polynomials and semi-empirical equations [61–63]. The phase equilibrium is determined by the Clausius–Clapeyron relation. The Westbrook–Dryer one-step oxidation kinetics [60] is used here for the gas-phase reaction. This use of the one-step mechanism for this droplet burning problem has been justified by Wu et al. [64]; they have shown using a four-step reduced kinetics model that a complete qualitative description and a good quantitative description result from the one-step approximation for the droplet burning problem. Note that this mechanism should not describe well the ignition problem.

5.2. Single-layer convective array results

The transient convective burning of n-octane droplets within several single-layer arrays in a hot air stream has been simulated with considerations of droplet regression, deceleration of the stream flow, liquid motion, variable properties, non-uniform surface temperature and surface tension. Infinite periodic arrays, semi-infinite periodic arrays with one row or two rows of droplets, and finite arrays with nine droplets with centers in a plane have been considered. Comparisons show that the interactions amongst droplets increases as the number of rows in the array increases. The transient flame shape, surface temperature, and burning rate were investigated under different initial parameters. The critical parameters for the determination of the initial flame shapes and the moment of wake-to-envelope transition for an initial wake flame were determined for all these arrays.

Fig. 11a–d shows the contours of the chemical reaction rate at two instants during the lifetime, for four cases with different initial relative stream velocity or initial droplet spacing. The initial flame shape is either an envelope flame or a wake flame, and either a connected flame, also known as a group flame, or a separated flame, as determined by the initial relative stream velocity and the initial droplet spacing. In the transient process, an initial envelope flame remains an envelope flame, and an initial wake flame has a tendency to develop from a wake flame to an envelope flame. The transition relates to the increasing surface temperature, decreasing Reynolds number (due to the decrease of both droplet radius and relative stream velocity), and increasing Damköhler number (due to the faster decrease of relative stream velocity than the droplet radius) over time, all of which favor an envelope flame. The flame standoff distance shows no strong tendency to be modified significantly during the lifetime of the droplet; i.e., an initially separated flame remains separated and an initially connected flame remains connected, unless the initial flame is too close to the critical state between a separated flame and a connected flame. This can be explained from the general balance of the regression of the droplet surface over time which tends to shrink the flame, and the decreasing Reynolds number and increasing surface temperature over time which tend to increase the flame stand-off. By themselves, the decrease of the Reynolds number and the increase of the surface temperature allow the fuel vapor to diffuse and advect farther from the droplet surface and thus increase the flame stand-off.

Wu and Sirignano identified that the droplet wake flames had a tri-brachial character which appears in many flameholding structures and are often named edge-flames. See, for example, the excellent review by Buckmaster [65]. In this class of flames, a stratified inflow has varying mixture ratio in a direction transverse to the flow through the flame front; consequently, these flames have a fuel-lean premixed-flame branch and a fuel-rich premixed-flame branch, followed by a diffusion-flame branch. Fig. 11b shows the tri-brachial character at the upstream edge of the wake flame.

Fig. 12(a,b) shows the instantaneous average surface temperature and normalized mass burning rate for the three types of arrays with the same initial droplet spacing $sp_0 = 2.4d_0$, at the initial Reynolds number $Re_0 = 5.5$ and 45, respectively. For $Re_0 = 5.5$ ($Da_0 = 2.4$) with an envelope flame during the lifetime, the increase of the surface temperature for the semi-infinite periodic array with one row of droplets is higher than the other two arrays due to a higher flame temperature resulting from less interaction amongst droplets and greater chemical reaction rate. For $Re_0 = 45$ ($Da_0 = 0.3$) with an initial wake flame, the wake-to-envelope transition during the lifetime is indicated by the sharp increase of the average surface temperature and the mass burning rate in Fig. 12(b). It was found in Ref. [40] that the moment of wake-to-envelope transition is advanced as the initial droplet spacing is decreased if the initial droplet spacing is not too small, due to an increase in the "velocity-decrease effect" as the interaction amongst droplets increases. A "velocity-decrease effect" means that the gas velocity between droplets is decreased as spacing deceases because the flow is cooled and density increases. In a similar behavior, the moment of wake-to-envelope transition is earliest for the infinite periodic array with the most interaction amongst droplets, and latest for the semi-infinite periodic array with one row of droplets with the least interaction amongst droplets. The mass burning rate for the three types of arrays is varied because of different interaction of fuel vapor amongst droplets and different time of wake-to-envelope transition for an initial wake flame. At $Re_0 = 5.5$ with an envelope flame all the time, the mass burning rate is greater for the arrays with smaller interaction of fuel vapor amongst droplets. At $Re_0 = 45$ for an initial wake flame, the mass burning rate is also influenced by the wake-to-envelope transition which elevates the surface temperature, and the array with more interaction amongst droplets (e.g., the infinite periodic array) may have greater mass burning rate for some period during the lifetime due to an earlier wake-to-envelope transition.

Wu and Sirignano [40] compare the behavior of semi-infinite periodic arrays and finite arrays with the behavior of previously studied infinite periodic arrays. Furthermore, the critical values of the initial Damköhler number are identified for bifurcations in flame behavior at various initial droplet spacing for all these arrays. For a given array configuration under specific initial droplet spacing and ambient conditions, there exists a critical initial Damköhler number below which the flame is initially wake flame and above

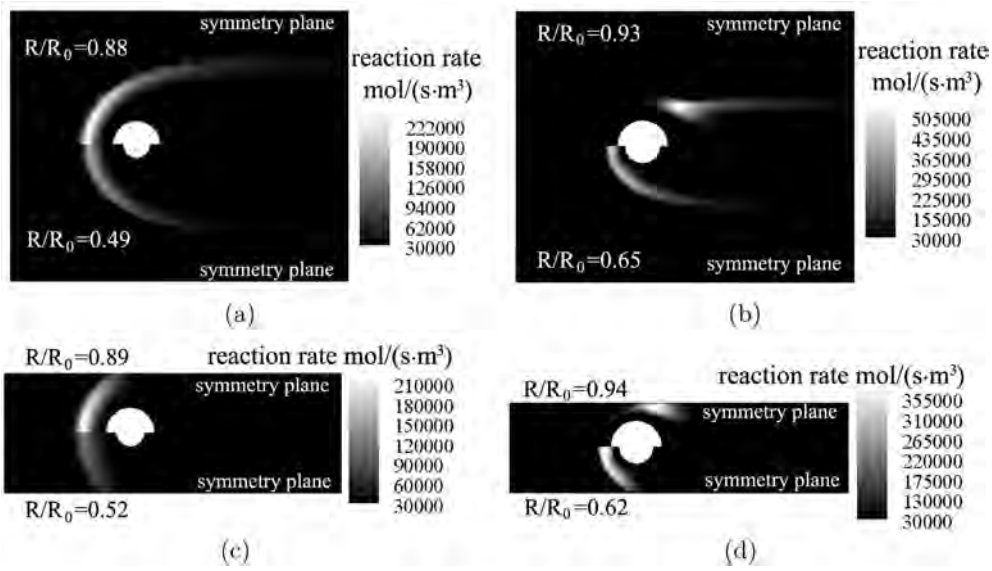

Fig. 11. The contours of the chemical reaction rate at two instants during the lifetime, for four cases: (a) $Re_0 = 9$ ($Da_0 = 1.5$) and $sp_0 = 5.9\ d_0$, with the initial flame shape envelope and separated; (b) $Re_0 = 45$ ($Da_0 = 0.3$) and $sp_0 = 5.9\ d_0$, with the initial flame shape wake and separated; (c) $Re_0 = 9$ ($Da_0 = 1.5$) and $sp_0 = 2.4\ d_0$, with the initial flame shape envelope and connected; (d) $Re_0 = 45$ ($Da_0 = 0.3$) and $sp_0 = 1.8\ d_0$, with the initial flame shape wake and connected [40].

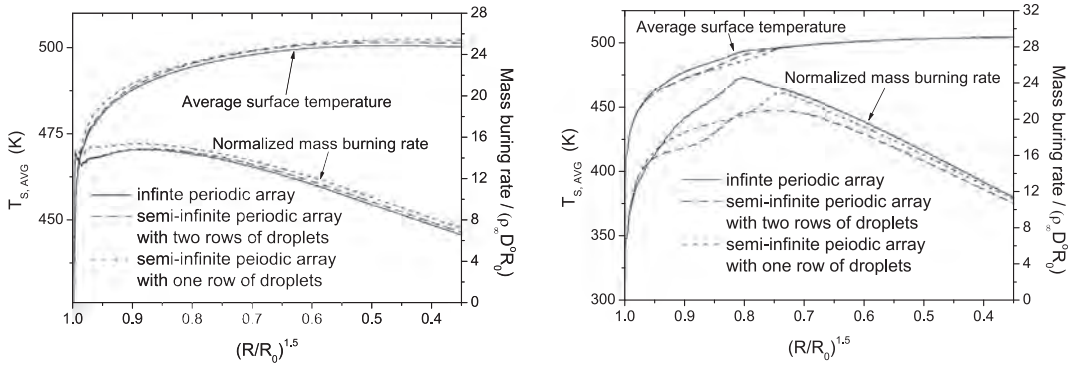

Fig. 12. The comparisons of the instantaneous average surface temperature and normalized mass burning rate for three different types of arrays (with the same initial droplet spacing $sp_0 = 2.4d_0$), at the initial Reynolds number $Re_0 = 5.5$ and 45, respectively [41]. (a) $Re_0 = 5.5$ ($Da_0 = 2.4$) (b) $Re_0 = 45$ ($Da_0 = 0.3$).

which the flame is initially envelope flame. For the initial Damköhler number below the critical value, the initial wake flame will be transitioned into an envelope flame later during the lifetime. The interaction amongst droplets at intermediate droplet spacing increases as the number of rows in the array increases. The interaction also increases as the initial droplet spacing decreases for a specific number of rows in the array. Consequently, the critical initial Damköhler number decreases and the moment of wake-to-envelope transition from an initial wake flame is advanced, both implying a preference for an envelope flame. The initial flame shape as either separated flames or a connected flame (group flame) is determined by the initial Reynolds number, initial Damköhler number and initial droplet spacing. An initial envelope flame can be an initial connected flame over a wider range of initial Reynolds number than an initial wake flame. The mass burning rate is influenced by the Reynolds number, interaction of fuel vapor amongst droplets, and the moment of wake-to-envelope transition for an initial wake flame. The array with more interaction amongst droplets may have greater mass burning rate for some period during the lifetime due to an earlier wake-to-envelope transition. Lower ambient pressure causes a later wake-to-envelope transition and smaller mass burning rate because of slower reaction kinetics.

Fig. 13 shows the values of the critical initial Damköhler number at different initial droplet spacing, for an infinite periodic array and a semi-infinite periodic array with one row of droplets, respectively. From the discussions for the moment of wake-to-envelope transition [40], the preference for an envelope flame is increased as the initial droplet spacing is decreased, but this trend is hindered as the initial droplet spacing becomes too small. Therefore, the critical initial Damköhler number becomes smaller (implying preference for an envelope flame) for decreasing initial droplet spacing when it is intermediate but has no substantial change when the initial droplet spacing becomes too small. The critical initial Damköhler number for a semi-infinite periodic array is generally greater than that for an infinite periodic array at the same initial droplet spacing, because the effective droplet spacing is actually greater for a semi-infinite periodic array with one row of droplets in which there are no droplet interactions in the other direction. We also investigated the initial flame shape as either separated or connected flame (group flame) determined by both

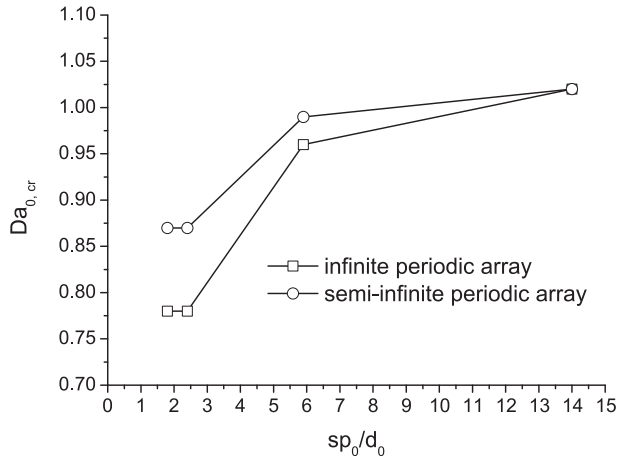

Fig. 13. The values of the critical initial Damköhler number (for the determination of whether the flame is initially wake or envelope flame) at different initial droplet spacing, for an infinite periodic array and a semi-infinite periodic array with one row of droplets, respectively [41].

initial Reynolds number and initial Damköhler number. Critical values of the initial Reynolds number (for the determination of an initial separated or connected flame) can be found for given initial Damköhler number and initial droplet spacing. Fig. 14 shows the critical initial Reynolds number at different initial Damköhler number at the initial droplet spacing $sp_0 = 2.4d_0$, for the two array configurations. For each array configuration, the solid curve of the critical Re_0 and the dashed vertical line of the critical Da_0 (for the determination of an initial wake or envelope flame) divide the plane into four domains, with the initial flame wake-separated for the left-upper corner, wake-connected for the left-lower corner, envelope-separated for the right-upper corner, and envelope-connected for the right-lower corner. It is found that the critical Re_0 increases as the flame is changed from an initial wake flame to an initial envelope flame, and does not change much in the initial envelope flame zone. This implies that an initial envelope flame can be an initial connected flame over a wider range of initial Reynolds number than an initial wake flame, as shown in Fig. 14.

For the array with nine droplets with centers in a plane (nine-droplet array), there are three different types of droplet positions:

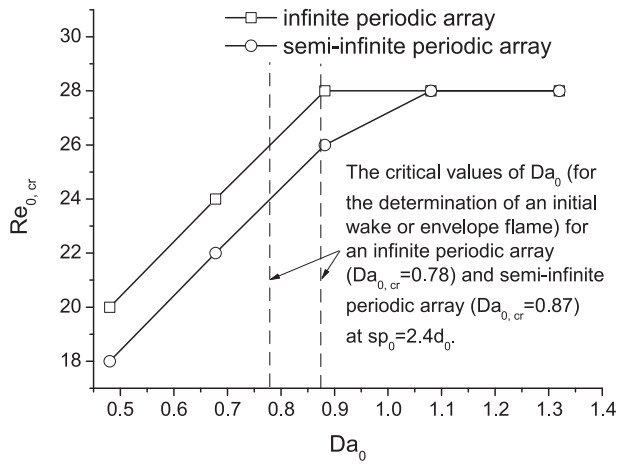

Fig. 14. The values of the critical initial Reynolds number (for the determination of whether the flame is initially separated or connected) at different initial Damköhler number under the same initial droplet spacing ($sp_0 = 2.4d_0$), for an infinite periodic array and a semi-infinite periodic array with one row of droplets, respectively [41].

at the plane center, at the edge center, and at the corner. The droplet at the plane center has the lowest vaporization rate for cases with a group envelope flame, but may have the greatest vaporization rate for cases with nine separated wake flames initially due to the earliest wake-to-envelope transition. The droplet at the plane center has the smallest critical initial Damköhler number, and the droplet at the corner has the greatest. The critical initial Damköhler number for the droplet at the plane center in a nine-droplet array is greater than that for a droplet in an infinite periodic array at the same initial droplet spacing. The initial flame shape as either a wake or envelope flame might be different for the three types of droplet positions in a nine-droplet array, due to the difference in the critical initial Damköhler number for the three types of droplet positions. The critical initial Damköhler number for the nine-droplet arrays is also found for the determination of whether the flame is initially wake or envelope flame. At the initial droplet spacing $sp_0 = 2.4d_0$, the critical initial Damköhler number is 0.84, 0.90, and 0.96 for the droplet at the plane center (droplet '1' in Fig. 10(a)), the droplet at the edge center (droplet '2' or '3'), and the droplet at the corner (droplet '4'), respectively. The droplet at the plane center with the strongest droplet interaction has the smallest critical initial Damköhler number, which is consistent with the earliest wake-to-envelope transition for an initial wake flame shown above. However, the critical initial Damköhler number for the droplet at the plane center is greater than the value (0.78) for a droplet in an infinite periodic array with the same initial droplet spacing, because the droplet in an infinite periodic array has even stronger droplet interaction. As the critical initial Damköhler number is different for the three types of droplet positions in a nine-droplet array, the initial flame shape as either a wake or envelope flame might be different for the three types of droplet positions. Fig. 15(a–d) shows the initial flame shapes (represented by the contours of chemical reaction rate at three cross-sections) for the nine-droplet arrays (with $sp_0 = 2.4d_0$) at different initial Reynolds number and initial Damköhler number. The initial flames are separated for the former three cases, while the initial flames are connected as a group flame for the last case with a low initial Reynolds number. At $Da_0 = 0.78$ which is smaller than the critical initial Damköhler number $Da_{0,cr}$ for all the three types of droplet positions, the initial flames are wake flames for all the droplets. At $Da_0 = 1.02$ which is greater than $Da_{0,cr}$ for all the three types of droplet positions, the initial flames are envelope flames for all the droplets. At $Da_0 = 0.90$, the droplet at the plane center with $Da_{0,cr} < 0.90$ has an initial envelope flame, while the droplet at the corner with $Da_{0,cr} > 0.90$ has an initial wake flame.

The instantaneous dimensionless numbers C_D, Nu, Sh, B_H, and B_M become close for various cases after a period of relaxation, when the liquid heating slows down and the relative spacing amongst droplets is increased. The cases for greater initial Reynolds number have generally greater B_H and B_M, but smaller C_D, Nu, and Sh at the same Re_m. This indicates that C_D, Nu, and Sh are inversely correlated to Spalding numbers, which is consistent to the results for an isolated droplet vaporization in the literature. The changes of the instantaneous Nu and B_M for various cases are characterized by the changes of the surface temperature.

5.3. Double-layer convective array results

The transient burning of convective *n*-octane droplets in a double-layer array was simulated numerically [42] by solving the Navier–Stokes, energy and species equations. The array is infinite in both cross-flow directions and has two droplet layers in the flow direction. Each layer in the double-layer array is a periodic droplet array of the same type discussed for single-layer arrays and the plane of the droplet centers for each layer is aligned orthogonal to

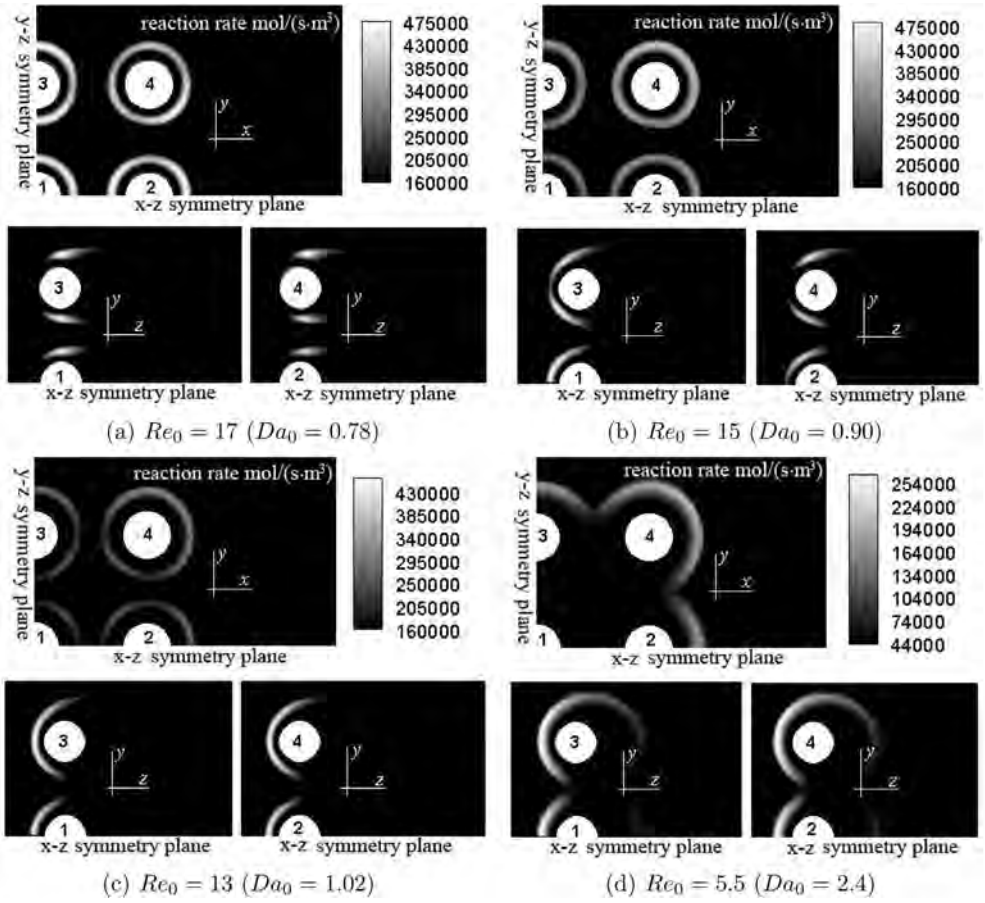

Fig. 15. The initial flame shapes (represented by the contours of chemical reaction rate at three cross-sections) for the nine-droplet arrays (with $sp_0 = 2.4d_0$) at different initial Reynolds number and initial Damköhler number [41]. (a) $Re_0 = 17$ ($Da_0 = 0.78$) (b) $Re_0 = 15$ ($Da_0 = 0.90$) (c) $Re_0 = 13$ ($Da_0 = 1.02$) (d) $Re_0 = 5.5$ ($Da_0 = 2.4$).

the free-stream velocity; so, the two layers are parallel with second layer further downstream. Fig. 16a and b shows the two types of droplet arrangement in the flow direction, i.e., droplets in tandem or staggered along the flow direction. The flow is in the z direction. For the staggered arrangement, the droplets are staggered not only in the x direction (as suggested in Fig. 16b), but also in the y direction. So, the two droplet centers in Fig. 16b are actually in different x–z planes for 3-D configurations. Each droplet represents a periodic distribution of droplets in the x–y plane by the use of y–z and x–z symmetry planes. Only two droplets need to be considered in the calculation with the proper use of symmetry planes. They are the front droplet (the representative droplet in the upstream layer) and back droplet (the representative droplet in the downstream layer). In fact, the actual domain for the calculation can be further reduced to include only a quarter of each droplet due to symmetries.

The transient behaviors for both front and back droplets and the relative movement between the two droplets were determined for various initial relative stream velocity and initial transverse droplet spacing. Droplet surface regression, deceleration of the stream flow due to the drag of the droplets, relative movement amongst droplets, internal circulation, variable properties, non-uniform surface temperature, and surface tension have been considered.

The calculations were first made for the assumption of no relative movement between front droplets (droplets in the upstream layer) and back droplets (droplets in the downstream layer) for droplets in tandem in different layers. However, due to different drags on the droplets in different layers, a relative movement

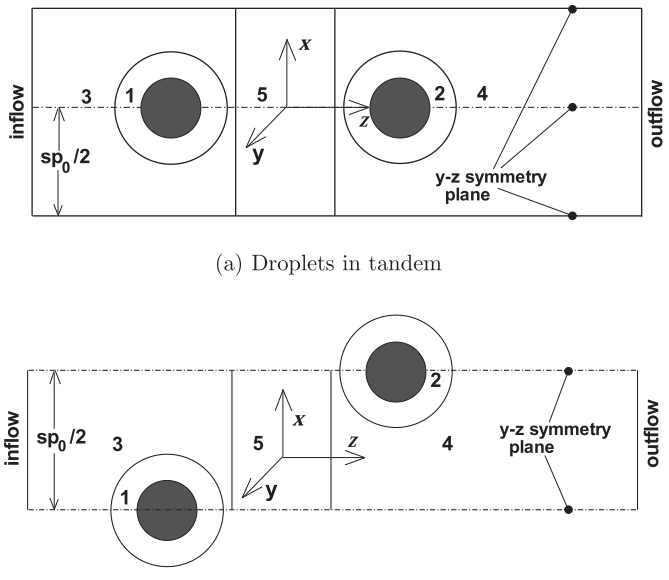

Fig. 16. The domains and boundaries of the double-layer periodic droplet array (displayed in the x–z plane), with the grey zones representing the liquid phase and the rest representing the gas phase, which is divided into five domains: spherical domains 1 and 2, and cartesian domains 3, 4, and 5 [42]. (a) Droplets in tandem (b) Staggered droplets.

between front droplets and back droplets is expected and thus considered in the later calculations for a better account of the real physics. The transient behaviors both for front droplets and back droplets are studied and compared, for various initial relative stream velocity and initial transverse droplet spacing. The droplets staggered in different layers are also studied, with a focus on the flame structures and relative movement between the front and back droplets.

While the studies of single-layer arrays only provided insights for the behaviors of the most upstream droplets in a real spray, the studies of double-layer arrays also help understand the behaviors of the downstream droplets more common in a real spray and, additionally, verify the representation of single-layer arrays for the most upstream droplets in a spray by the comparisons of the behaviors of the single-layer arrays and the upstream droplets in double-layer arrays. The model and code are expanded accordingly to allow the relative movement between the front and back droplets. Therefore, the studies of double-layer arrays are a big step toward understanding the totality of the behaviors of a real spray. No previous analysis has resolved the transient flow and transport for both the surrounding gas and the internal liquid of a burning droplet array with relative motion between droplets.

There are three different flame structures for the configuration of droplets in tandem: an envelope flame around both front droplet and back droplet, envelope flame for the back droplet but wake flame for the front droplet, and wake flame only behind the back droplet. One more flame structure, i.e., wake flames behind both front and back droplets exists for the configuration of staggered droplets. The initial flame structure is influenced by the initial Reynolds number (or initial Damköhler number) and the initial streamwise droplet spacing. When the initial streamwise droplet spacing is sufficiently large compared to initial droplet radius R_0 (e.g., $10.6R_0$) for the droplets in tandem, the back droplet will have an initial envelope flame even at a large initial Reynolds number or small initial Damköhler number (e.g., $Re_0 = 110$, $Da_0 = 0.12$).

The air flow has velocity U_∞, pressure p_∞, and temperature T_∞. The initial droplet temperature $T_{s,0}$ is uniform and low compared to the boiling point. The droplets have the same initial radius R_0. The transverse droplet spacing (in the x–y plane) is sp_0 for both layers. The streamwise droplet spacing (in the z direction) is initially $s_{z,0}$ and might change with time because of the expected relative movement between the two layers of droplets. Although the front droplet has a time-varying velocity $U_{d,1}$, we consider that it is not moving by instantaneously having an inertial frame of reference moving at the velocity of the front droplet [30,31,52]. The relative stream velocity becomes: $U'_\infty = U_\infty - U_{d,1}$. The back droplet might move relatively to the front droplet with a velocity of $U'_{rel} = U_{d,2} - U_{d,1}$. A positive value of U'_{rel} means that the back droplet is moving toward to the front droplet. As the droplets are slowed by the drag, the relative stream velocity and the relative moving velocity of the back droplet are updated continuously. We assume that there is no relative movement amongst droplets in the cross-flow directions because of the balanced forces inside a periodic droplet array. The gas flow is laminar because the initial Reynolds number considered in this study is not large (below 150).

The gas-phase continuity, momentum, energy and species equations and liquid-phase continuity, momentum and energy equations are coupled and solved simultaneously. The equations are the same as those used in section 5.1. Because the front droplet is treated as stationary by instantaneously having an inertial frame of reference moving at the velocity of the front droplet while the back droplet has relative movement to the front droplet, the liquid–gas interface for the back droplet is moving in the z direction at the speed of U'_{rel}, which modifies the velocity boundary conditions at the droplet surface for the gas-phase spherical domain of the back droplet.

The droplets are slowed by the drag $C_{D,i}$ ($i = 1$ or 2) in the transient process, including pressure drag, friction drag and thrust drag. The instantaneous velocity of each of the droplets is thus determined by $(d\overline{U}_{d,i}/d\bar{t}) = (3/8)(1/\overline{\rho}_l)(\overline{U}^2_\infty/\overline{R}_i)C_{D,i}$, with $(d\overline{U}_{d,1}/d\bar{t}) = -(d\overline{U}'_\infty/d\bar{t})$.

At each time step, the momentum equations, energy equation and species equations (gas phase only) are solved in order for each domain (two liquid-phase spherical domains, two gas-phase spherical domains, and three gas-phase cartesian domains). The radius of each droplet, the relative velocity between the front droplet and the stream, and the relative velocity between the front and back droplets are updated instantaneously after each time step. The liquid phase is initially stationary with a uniform temperature $T_{s,0}$. The gas phase has initial conditions obtained from solving the non-temporal form of the governing equations at specific inflow conditions of p_∞, T_∞ and $U'_{\infty,0}$ without droplet heating, vaporization, and deceleration.

5.3.1. Fixed relative positions for droplets in tandem

First, we consider that there is no relative movement between the front and back droplets for the configuration of droplets in tandem. The initial flame shape should not be influenced by the relative movement between the front and back droplets which is negligible in the early period during the droplet lifetime. Although the transient behaviors are influenced by the relative movement between the front and back droplets, the transient results without the consideration of the relative movement still deserve to be studied because there can be some experimental situation with suspended droplets in tandem which don't move with respect to each other.

The initial flame shape can be illustrated by the contours of the gas-phase reaction rate and temperature at an early instant during the lifetime. Fig. 17a–h shows the contours for four cases: case 1 with $Re_0 = 11$ and $s_{z,0} = 5.6R_0$, case 2 with $Re_0 = 45$ and $s_{z,0} = 5.6R_0$, case 3 with $Re_0 = 110$ and $s_{z,0} = 5.6R_0$, and case 4 with $Re_0 = 110$ and $s_{z,0} = 10.6R_0$. All the cases have the same initial transverse droplet spacing $sp_0 = 5.9d_0$. Cases 1, 2 and 3 have the same streamwise droplet spacing $s_{z,0} = 5.6R_0$ but increasing initial Reynolds number (or decreasing initial Damköhler number). Therefore, case 1 with low initial Reynolds number has an envelope flame around both front droplet and back droplet; case 2 with greater initial Reynolds number has a wake flame for the front droplet but an envelope flame for the back droplet; and case 3 with further greater initial Reynolds number has a wake flame for the back droplet with limited burning forward of the back droplet. As the streamwise droplet spacing is increased from $5.6R_0$ to $10.6R_0$ at the same initial Reynolds number $Re_0 = 110$, the initial flame shape for the back droplet changes from a wake flame (case 3) to an envelope flame (case 4). This occurs because the case with greater streamwise droplet spacing has greater characteristic length, greater residence time, and thus greater initial Damköhler number.

5.3.2. Relative movement for droplets in tandem

The relative movement between the front and back droplets is considered in this part for the tandem-droplet configuration. It is known [30,66] that the back droplet approaches the front droplet rapidly for the same initial droplet diameter. With this expectation, the calculation [42] begins with an initial streamwise droplet spacing in the order of $10R_0$, and is stopped when the streamwise droplet spacing is decreased to $4.0R_0$, below which the current model can not be handled with satisfactory accuracy.

The transient behaviors of the front droplet and back droplet are compared in Fig. 18 at the initial transverse droplet spacing

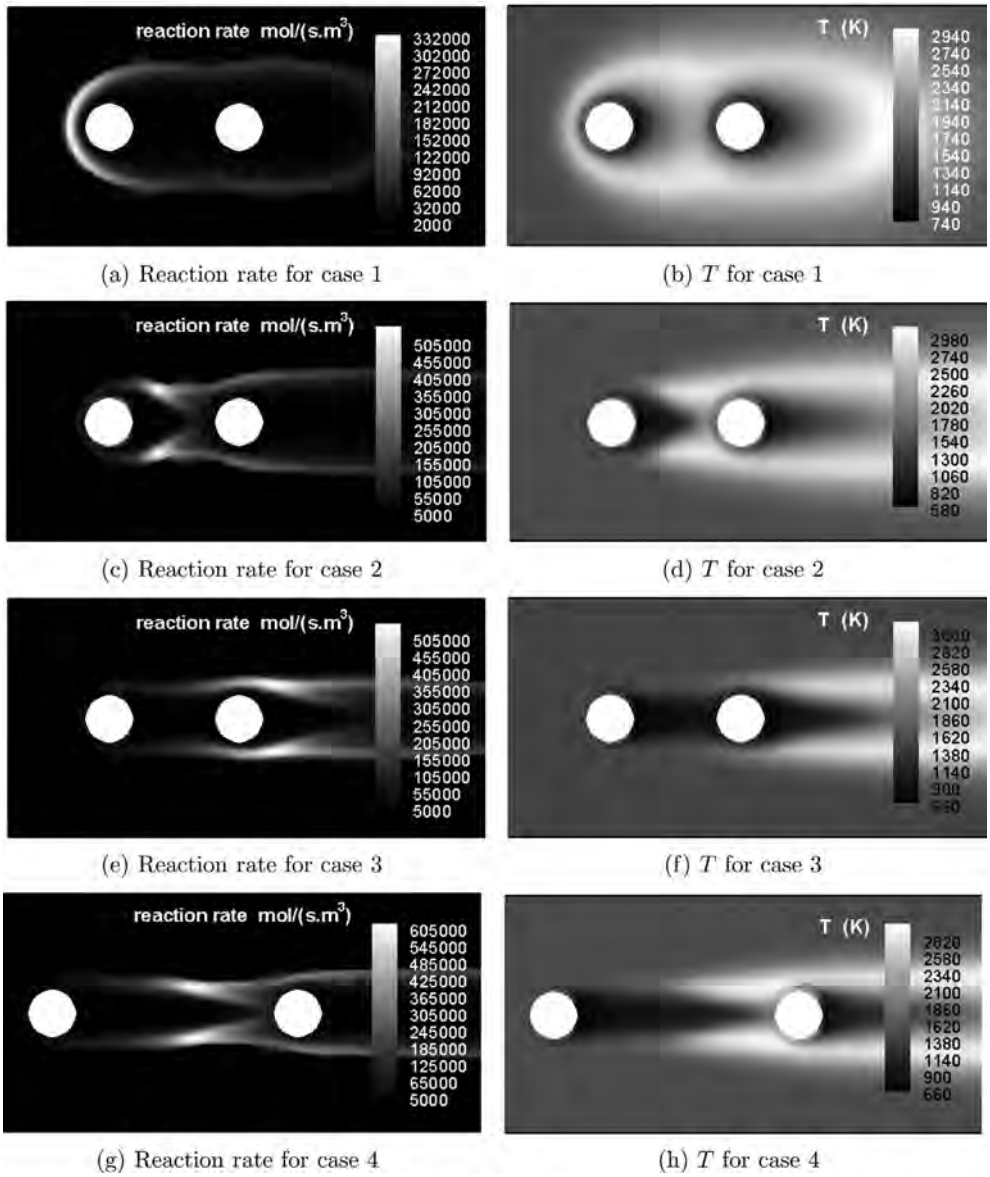

Fig. 17. The contours of the gas-phase reaction rate and temperature at an early instant during the lifetime for four cases: case 1 with $Re_0 = 11$ and $s_{z,0} = 5.6R_0$, case 2 with $Re_0 = 45$ and $s_{z,0} = 5.6R_0$, case 3 with $Re_0 = 110$ and $s_{z,0} = 5.6R_0$, and case 4 with $Re_0 = 110$ and $s_{z,0} = 10.6R_0$. All the cases have the same initial transverse droplet spacing $sp_0 = 5.9d_0$ [42]. (a) Reaction rate for case 1 (b) T for case 1 (c) Reaction rate for case 2 (d) T for case 2 (e) Reaction rate for case 3 (f) T for case 3 (g) Reaction rate for case 4 (h) T for case 4.

$sp_0 = 5.9d_0$ and the initial Reynolds number $Re_0 = 11$. The initial streamwise droplet spacing is $s_{z,0} = 10.6R_0$. There is an initial envelope flame around both droplets in this case. The back droplet has lower drag than the front droplet because the flow is decelerated by the front droplet before reaching the back droplet. Therefore, the back droplet has greater velocity and is moving toward the front droplet, and the streamwise distance between the two droplets decreases continuously during the transient process (Fig. 18b and e). The plateau or slight decease in the relative velocity between the two droplets after a period of fast increase (Fig. 18e) can be explained by an elevation of the drag on the back droplet due to its fast movement toward the front droplet. For the flame structure with an envelope flame around both droplets, the front droplet is better enclosed by the flame than the back droplet (Fig. 17a and b). So, the front droplet has higher average surface temperature and greater overall vaporization rate than the back droplet (Fig. 18a, c and d). For smaller transverse droplet spacing at which the flame forward of the front droplet does not stretch toward the back droplet, the differences of the surface temperature and vaporization rate between the front droplet and back droplet are more significant.

The transient behaviors of the front droplet and back droplet are also compared at the initial transverse droplet spacing $sp_0 = 2.4d_0$ and a greater initial Reynolds number $Re_0 = 45$. The initial streamwise droplet spacing is still $s_{z,0} = 10.6R_0$. The initial flame is an envelope flame for the back droplet but a wake flame for the front droplet. So, the front droplet has a lower average surface temperature than the back droplet for a long time until the wake flame is transitioned into an envelope flame for the front droplet (Fig. 19a). The lower average surface temperature for the front droplet also results in a smaller vaporization rate than the back droplet before the wake-to-envelope transition (Fig. 19c and d). From Fig. 19e, the back droplet is moving toward the front droplet at a greater speed compared to the case with smaller initial

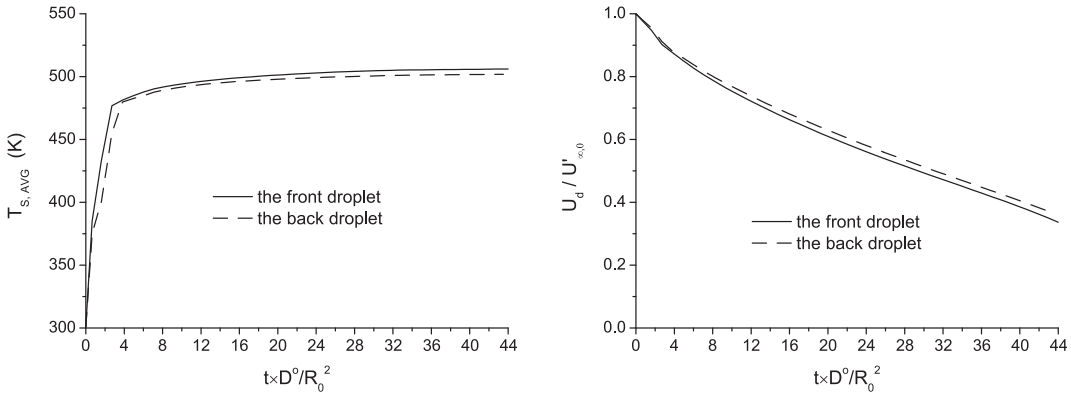

(a) Average surface temperature

(b) Normalized droplet velocity

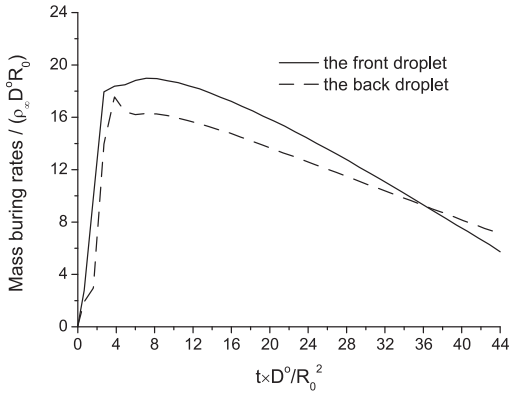

(c) Mass burning rates

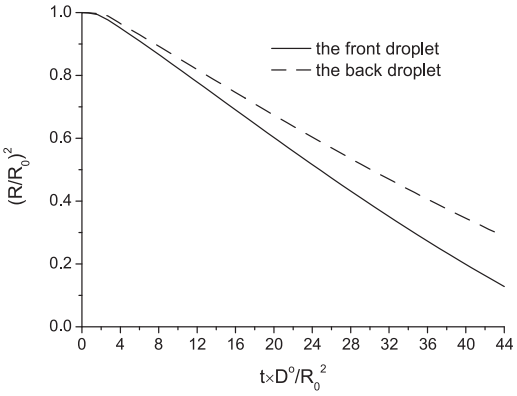

(d) Normalized radius squared

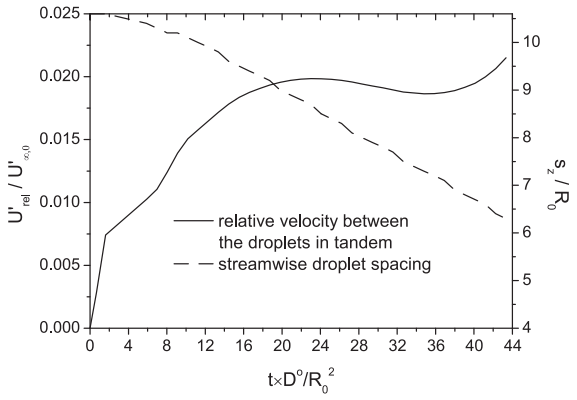

(e) Relative velocity and streamwise distance between the two droplets

Fig. 18. The comparisons of the instantaneous quantities between the front droplet and the back droplet, and the relative velocity and streamwise distance between the two droplets in tandem, at the initial transverse droplet spacing $sp_0 = 5.9d_0$ and the initial Reynolds number $Re_0 = 11$ [42]. (a) Average surface temperature (b) Normalized droplet velocity (c) Mass burning rates (d) Normalized radius squared (e) Relative velocity and streamwise distance between the two droplets.

Reynolds number. So, the streamwise distance between the two droplets decreases rapidly and collision is possible before a major fraction of the droplet volume has been vaporized.

In the calculation with fixed spacing between the two droplets in tandem, the front droplet in a double-layer array behaves similarly to the droplet in a single-layer array for the streamwise droplet spacing of $10.6R_0$ and $5.6R_0$ considered. This result is also expected for the cases with consideration of relative movement between the two droplets in tandem. To verify this, we compare the transient behaviors of the front droplet amongst three cases: the case with relative movement between the two droplets in tandem with $s_{z,0} = 10.6R_0$, the case with constant $s_z = 10.6R_0$, and the case with constant $s_z = 5.6R_0$, at the condition of $sp_0 = 5.9d_0$ and $Re_0 = 11$, or $sp_0 = 2.4d_0$ and $Re_0 = 45$, respectively. The results in

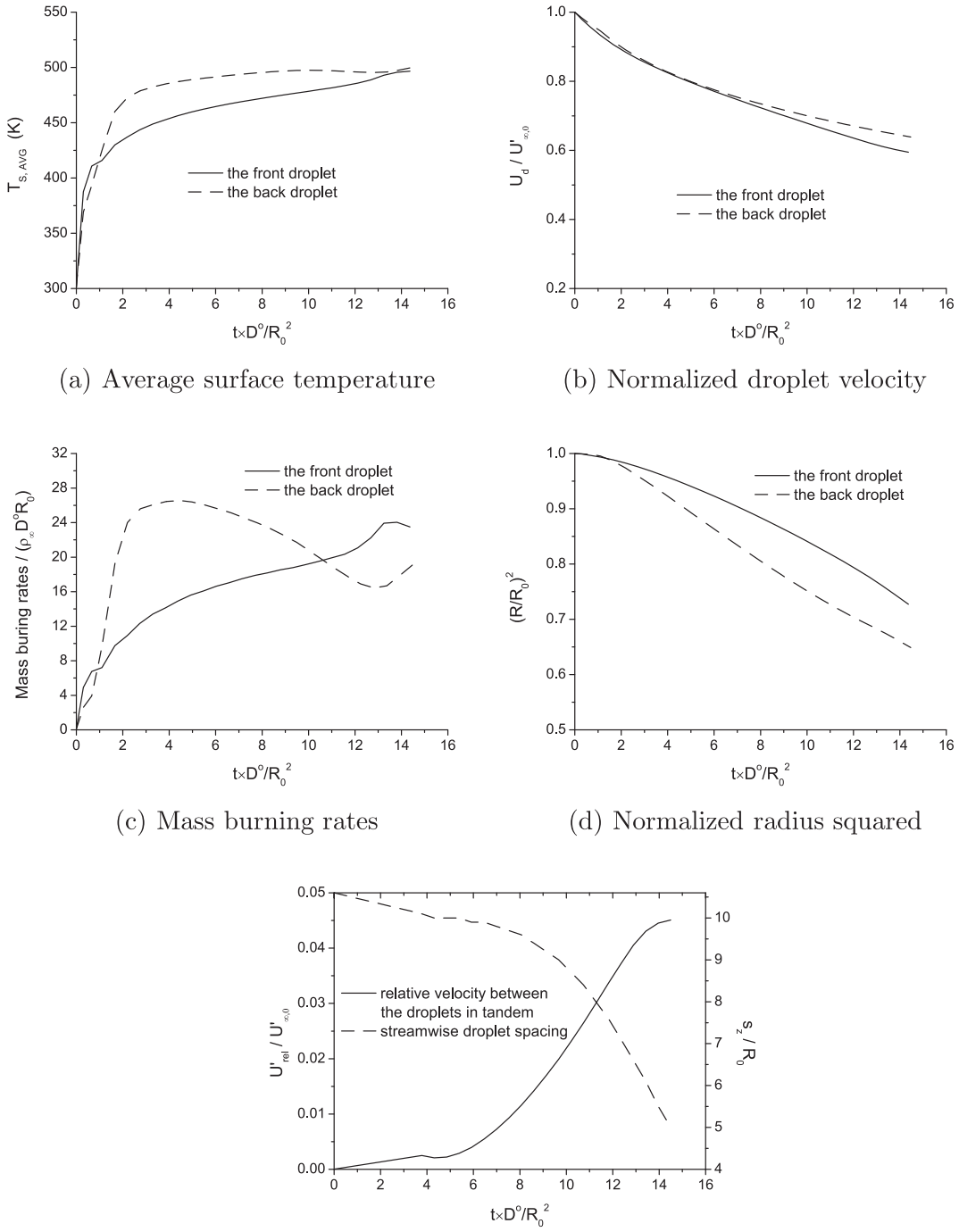

Fig. 19. The comparisons of the instantaneous quantities between the front droplet and the back droplet, and the relative velocity and streamwise distance between the two droplets in tandem, at the initial transverse droplet spacing $sp_0 = 2.4d_0$ and the initial Reynolds number $Re_0 = 45$ [42]. (a) Average surface temperature (b) Normalized droplet velocity (c) Mass burning rates (d) Normalized radius squared (e) Relative velocity and streamwise distance between the two droplets.

Fig. 20 show that the transient behaviors of the front droplet with s_z decreasing from $10.6R_0$ is close to the transient behaviors of the front droplet at both constant $s_z = 10.6R_0$ and constant $s_z = 5.6R_0$. So, the consideration of the relative movement between the two droplets in tandem does not influence the behaviors of the front droplet much, and the similarity of the front droplet in a double-layer array to the droplet in a single-layer array is still valid.

The behavior of the front droplet in a double-layer array is similar to the droplet in a single-layer array at other transverse droplet spacing; thereby, the effect of the transverse droplet spacing for the front droplet in a double-layer array is also similar to the behavior of a droplet in a single-layer array [40,41]. For the back droplet, the initial flame is an envelope flame for the highest initial Reynolds number of 110 considered in this study at the initial

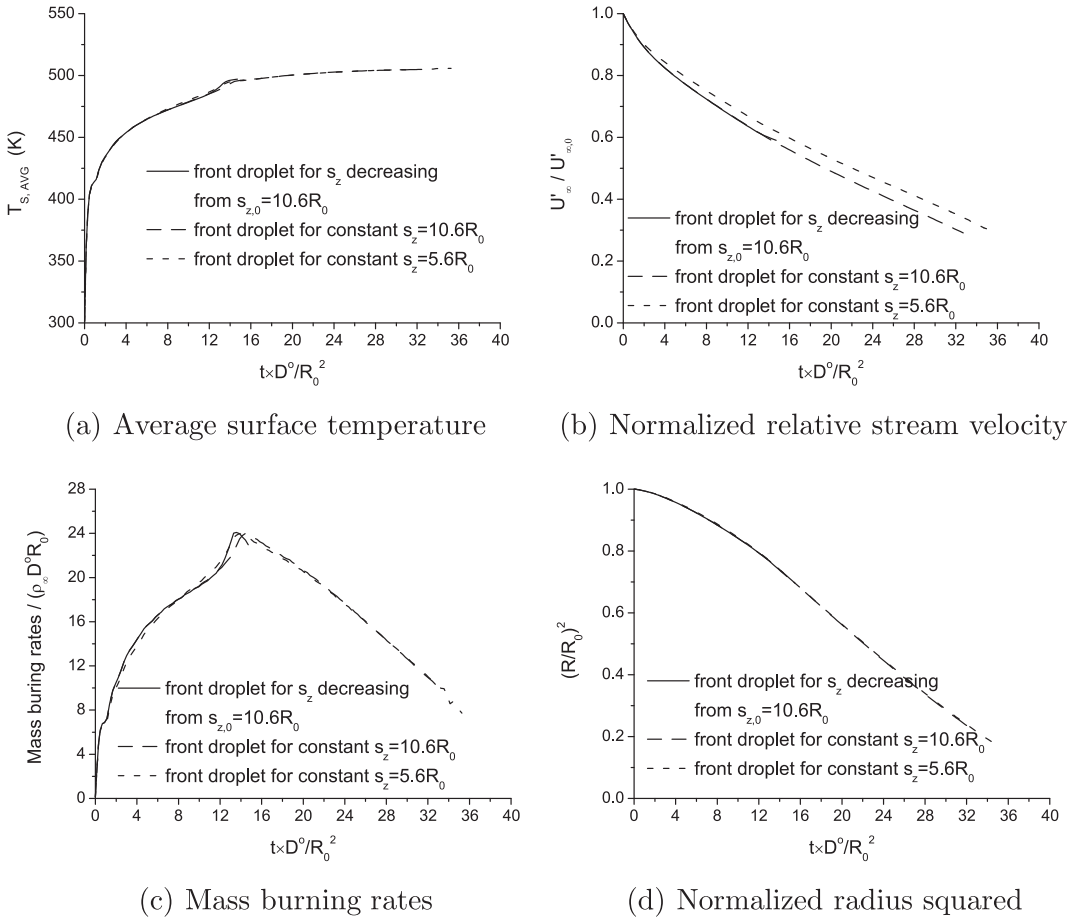

Fig. 20. The comparisons of the instantaneous quantities for the front droplet amongst three cases: the case with relative movement between the two droplets in tandem with $s_{z,0} = 10.6R_0$, the case with constant $s_z = 10.6R_0$, and the case with constant $s_z = 5.6R_0$. The initial transverse droplet spacing is $sp_0 = 2.4d_0$ and the initial Reynolds number is $Re_0 = 45$ [42]. (a) Average surface temperature (b) Normalized relative stream velocity (c) Mass burning rates (d) Normalized radius squared.

streamwise droplet spacing of $10.6R_0$. For an initial envelope flame, the case with smaller transverse droplet spacing has lower average surface temperature and smaller burning rate due to stronger interactions amongst droplets, as indicated from the results for the droplet in a single-layer array. This is also true for the back droplet in a double-layer array, as shown in Fig. 21a,c and d at a typical condition of $s_{z,0} = 10.6R_0$ and $Re_0 = 11$. Fig. 21b also shows that the decrease of the droplet velocity is slower for smaller transverse droplet spacing when it is intermediate, which is consistent with the results for the droplet in a single-layer array. These results are also applicable for other higher initial Reynolds number considered in this study (Fig. 22 for $Re_0 = 45$).

5.3.3. *Relative movement for staggered droplets*

Now, the configuration of staggered droplets is examined, with consideration of the relative movement between the front and back droplets. The staggered droplets resemble better the stochastic droplet distribution in a spray. As the droplets in different layers are staggered rather than in tandem, the back droplet is not directly in the wake of the front droplet. Therefore, the difference of the drag for the front and back droplets and the relative movement between the two droplets are not as significant as those for the configuration of droplets in tandem.

Again, there are three different flame structures for the configuration of droplets in tandem: an envelope flame around both front droplet and back droplet, envelope flame for the back droplet but wake flame for the front droplet, and wake flame only behind the back droplet. For the configuration of staggered droplets, there is another flame structure, i.e., wake flames behind both back droplet and front droplet, as displayed in Fig. 23a and b for the case with $Re_0 = 45$, $sp_0 = 3.8d_0$ and $s_{z,0} = 5.6R_0$. Fig. 24a and b compares the temporal average surface temperature and mass burning rate for the front and back droplets for this case. The back droplet has obviously earlier wake-to-envelope transition than the front droplet. The flame structure of wake flames behind both front and back droplets does not exist for the droplets in tandem (with intermediate streamwise droplet spacing) because a wake flame behind the front droplet automatically results in a flame in the front region of the back droplet (i.e., an envelope flame for the back droplet).

The temporal streamwise droplet spacing is compared in Fig. 25 for the following cases with different initial transverse droplet spacing or initial Reynolds number: $sp_0 = 2.1d_0$ and $Re_0 = 11$; $sp_0 = 2.1d_0$ and $Re_0 = 45$; $sp_0 = 3.8d_0$ and $Re_0 = 11$; $sp_0 = 3.8d_0$ and $Re_0 = 45$. The initial streamwise droplet spacing is $s_{z,0} = 5.6R_0$ for all the cases. The cases with an initial envelope flame for the front droplet ($Re_0 = 11$) have generally monotonic decrease of the streamwise droplet spacing. For the cases with initial wake flames ($Re_0 = 45$), the streamwise droplet spacing reaches a peak value first but then decreases monotonically. A period of increasing streamwise droplet spacing occurs due to the flow acceleration between the front droplets increasing the drag on the back droplets. After the back staggered droplet becomes a greater distance behind the front droplet, it experiences a decreased drag because of

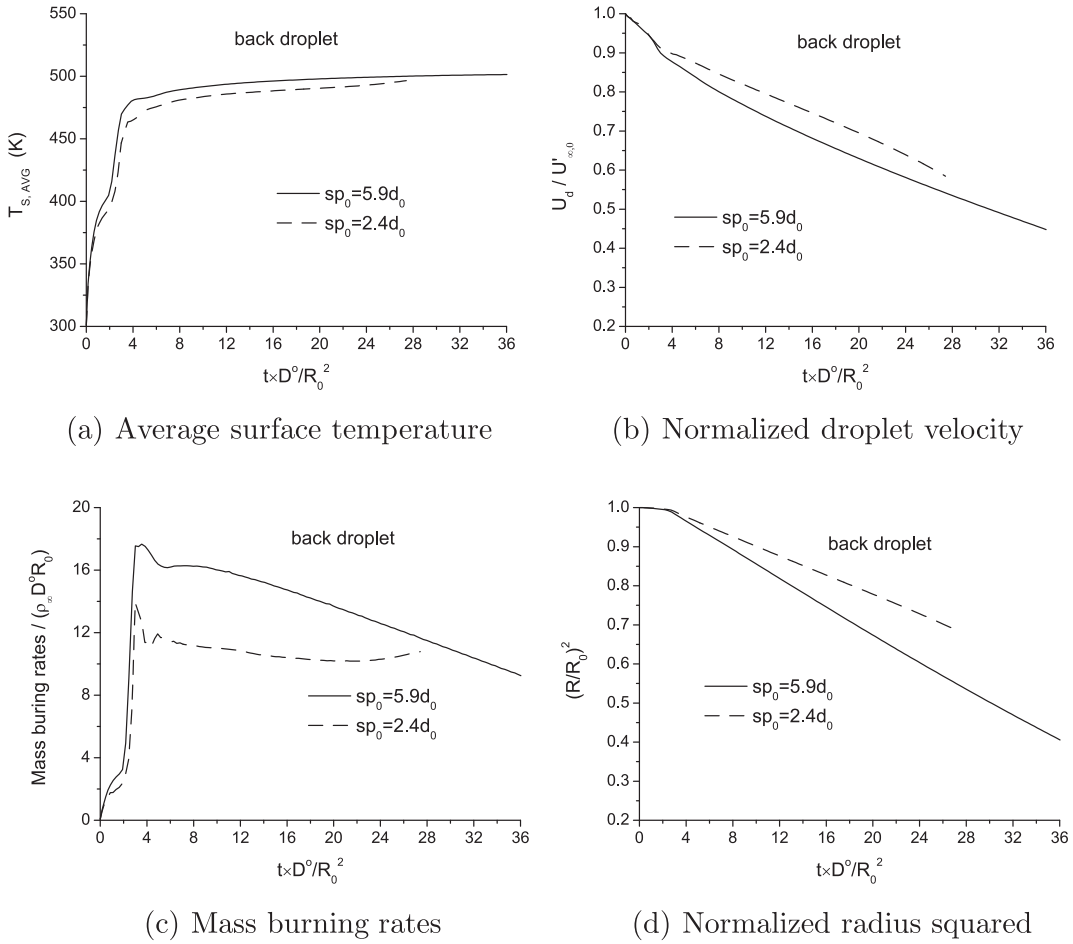

Fig. 21. The comparisons of the instantaneous quantities for the back droplet between the cases with different transverse droplet spacing of $sp_0 = 5.9d_0$ and $sp_0 = 2.4d_0$, at the initial streamwise droplet spacing $s_{z,0} = 10.6R_0$ and initial Reynolds number $Re_0 = 11$ [42]. (a) Average surface temperature (b) Normalized droplet velocity (c) Mass burning rates (d) Normalized radius squared.

the wake of the front droplet and then it moves forward more rapidly than the front droplet. The cases with smaller initial transverse droplet spacing ($sp_0 = 2.1d_0$) have faster decrease of the streamwise droplet spacing because they are closer to the configuration of droplets in tandem.

The front droplet in a double-layer array behaves similarly to the droplet in a single-layer array for the streamwise droplet spacing considered in this study, no matter whether the relative movement between the two droplets in tandem is allowed or not. So, the effect of the transverse droplet spacing for a droplet in a single-layer array is also applicable for the front droplet in a double-layer array. For the configuration of droplets in tandem, the back droplet has an initial envelope flame for most cases considered in this study, and smaller transverse droplet spacing yields lower average surface temperature and smaller burning rate due to stronger interactions amongst droplets, also similar to the results for the droplet in a single-layer array.

For droplets in tandem, the back droplet maintains a greater velocity and is moving toward the front droplet because it has lower drag than the front droplet. When the initial Reynolds number is high, the relative velocity between the two droplets in tandem might be fast and collision is expected before a major fraction of the droplet volume has been vaporized. For staggered droplets, the relative movement between the front and back droplets is not as significant as for droplets in tandem. There can be a period of increasing streamwise droplet spacing for the cases with initial wake flames due to the flow acceleration between the front droplets increasing the drag on the back droplets. If there is an initial envelope flame around both front and back droplets, the front droplet has higher average surface temperature and greater overall vaporization rate than the back droplet. If the initial flame is an envelope flame for the back droplet but a wake flame for the front droplet, the front droplet has lower average surface temperature and smaller vaporization rate than the back droplet before the wake-to-envelope transition for the front droplet. The configuration of staggered droplets has also initial wake flames for both front and back droplets, and the back droplet has earlier wake-to-envelope transition than the front droplet.

There are a limited number of experiments on vaporization of arrays with a relative motion between the droplets and gas. Some turbulent flow experiments will be discussed in the last section. For laminar flows, Nohara et al. [67] studied ignition of a linear array of decane droplets in a high-temperature low-speed air flow. In similar qualitative fashion to the computational results of Wu and sirignano, they found that the flame could first be established as a wake flame and then move forward in time over the droplet. The experiment showed that droplet spacing affected ignition delay.

5.4. Summary of convective burning of fuel-droplet arrays

Three-dimensional calculations for convective burning were conducted, accounting for temporal changes in droplet size,

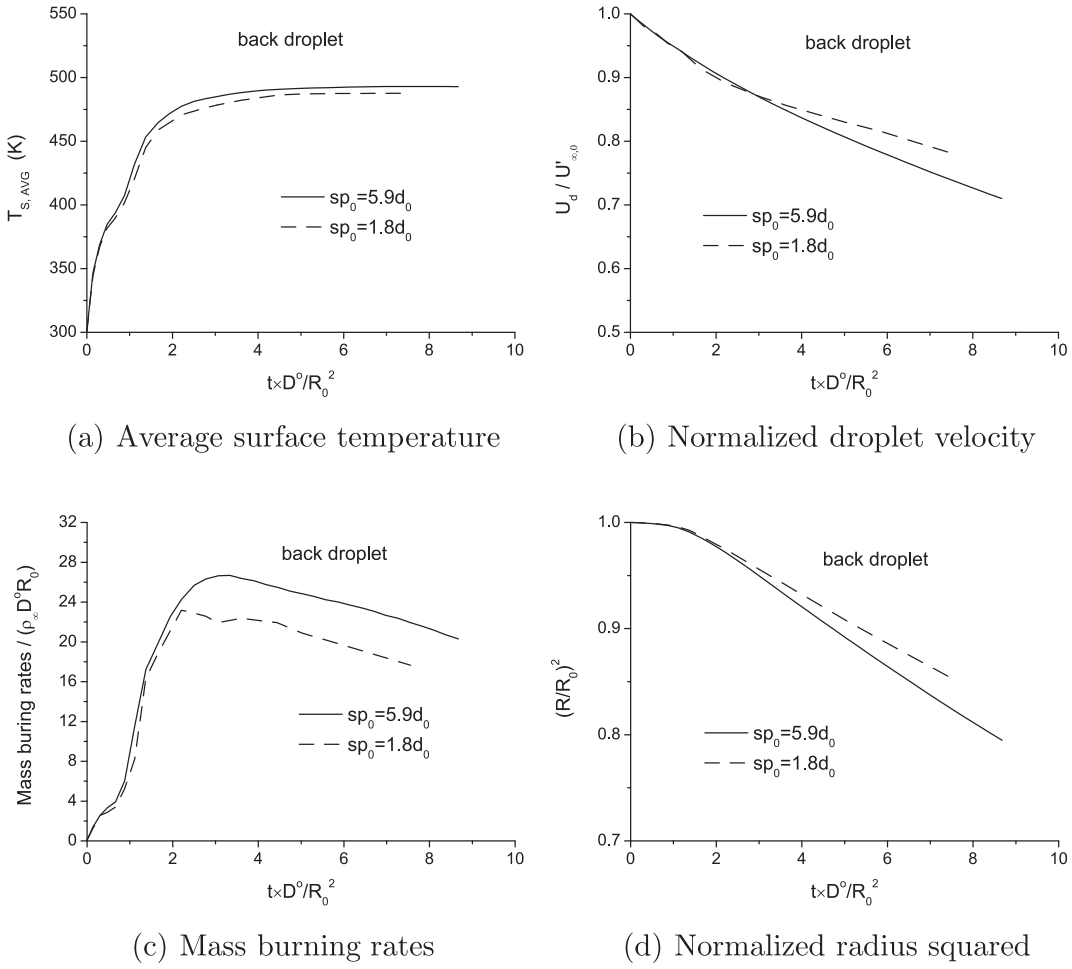

Fig. 22. The comparisons of the instantaneous quantities for the back droplet between the cases with different transverse droplet spacing of $sp_0 = 5.9d_0$ and $sp_0 = 1.8d_0$, at the initial streamwise droplet spacing $s_{z,0} = 10.6R_0$ and initial Reynolds number $Re_0 = 45$ [42]. (a) Average surface temperature (b) Normalized droplet velocity (c) Mass burning rates (d) Normalized radius squared.

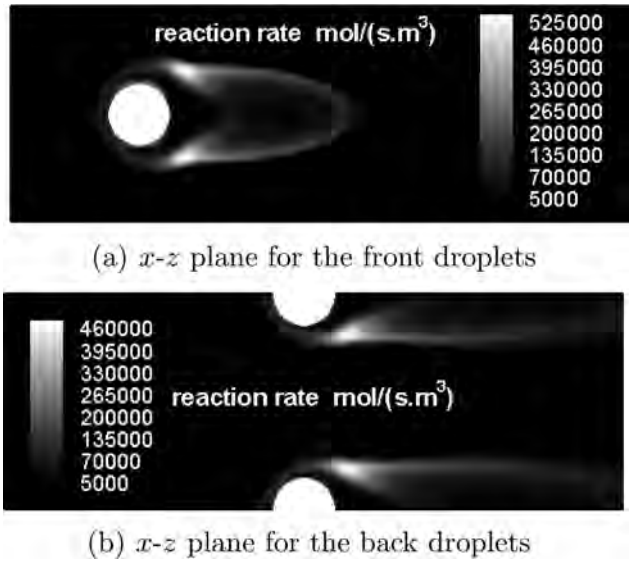

Fig. 23. The contours of the gas-phase reaction rate at an early instant during the lifetime for the staggered array case with $Re_0 = 45$, $sp_0 = 3.8d_0$ and $s_{z,0} = 5.6R_0$. The contours are displayed in two planes: (a) the x–z plane in which the centers of the front droplets are located, (b) the x–z plane in which the centers of the back droplets are located [42]. (a) x–z plane for the front droplets (b) x–z plane for the back droplets.

spacing, velocity, and temperature. These calculations directly hold no advantage for sub-grid modeling because dimensionality or the number of equations are not reduced. However, these approaches do hold promise for the development of correlations that will be useful in sub-grid modeling.

Forced convection causes major changes to flame modes, burning rates, and vaporization rates. The possible modes include individual envelope flames for each droplet, individual wake flames where flames are held in the downstream boundary layer or near wake of each droplet, envelope flames surrounding more than one droplet (group envelope flame), and merged wake flames for more than one droplet (group wake flame). In the transient process, modes can change. An individual or group envelope flame remains unchanged. However, an individual or group wake flame can develop into an envelope flame as the droplet decelerates relative to surrounding gas, increasing residence time for mixing and chemistry. Generally, individual flames remain as individual flames whether they start as envelope or wake flames and group flames also stay as group flames in transition from wake flames to envelope flames.

The flame standoff distance from the forward stagnation point for individual envelope flames remain almost unchanged as droplet decrease in size and relative velocity. The effects of size decrease and velocity decrease apparently cancel each other. The time of transition from wake flame to envelope flame advances first as

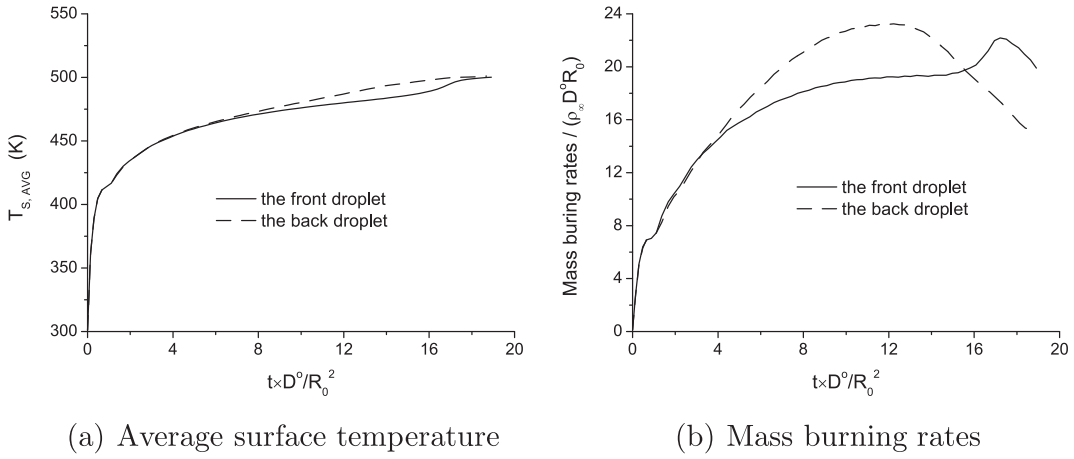

Fig. 24. The comparisons of the temporal average surface temperature and mass burning rate between the front droplet and the back droplet for the staggered array case with $Re_0 = 45$, $sp_0 = 3.8d_0$ and $s_{z,0} = 5.6R_0$ [42]. (a) Average surface temperature (b) Mass burning rates.

droplet spacing decreases but then delays with further decrease of spacing. Wake flames were found to have a tri-brachial character at the upstream end near the droplet.

Substantial deviations from a d^2 law were observed due to droplet spacing, finite Reynolds number, and transient heating and vaporization. In the double-layer case, significant differences in the burning rates of front and back droplets were found for both the tandem array and the staggered array.

There is a critical Damköhler number for determination of initial envelope or wake flame structure. This critical number does not vary with Reynolds number and decreases for decreasing spacing in an intermediate range. For small spacing, the critical number remains approximately constant. Lower ambient temperature decreases reaction rate, yielding lower Damköhler number, heating rates, and vaporization rates. This delays the transition time from wake flame to envelope flame. Lower ambient pressure decreases boiling point temperature and surface temperature; burning rate is lowered and transition is delayed.

Generally, an increase in Reynolds number implies thinner boundary layers and increased transport rates, thereby increasing burning rates. For transitional situations, the decrease in velocity that yields a lower Reynolds number can increase residence time, allowing an earlier transition to envelope flame with increased global burning rate.

For the double-layer case, the rear droplets decelerated at a lower rate than the front droplet; so, they moved faster than the front droplet which could lead to collisions. For the back droplets in the staggered case, the deceleration was greater and the velocity difference with the front droplet was smaller than found for the tandem case. The back droplets experienced wake-to-envelope flame transition earlier than the front droplets.

Extensions to cases with multicomponent fuels and/or spatially varying droplet initial size and spacing remain to be examined. A methodology for developing useful correlations for sub-grid models is also needed. Additional experimentation for cases where Kolmogorov scales and droplet sizes have the same order of magnitude are desired.

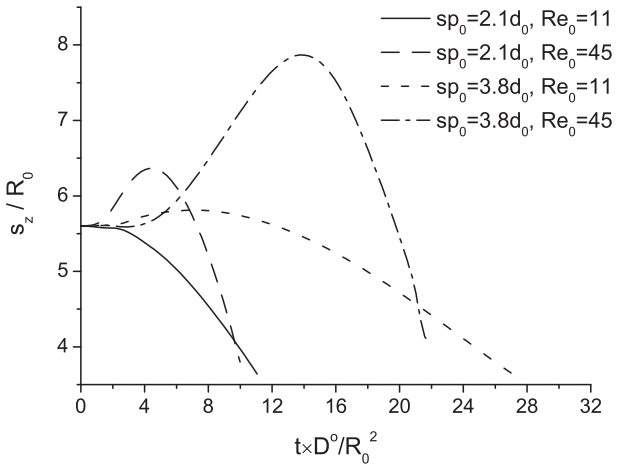

Fig. 25. The temporal streamwise droplet spacing for the staggered droplets with $s_{z,0} = 5.6R_0$, for the following four cases: $sp_0 = 2.1d_0$ and $Re_0 = 11$; $sp_0 = 2.1d_0$ and $Re_0 = 45$; $sp_0 = 3.8d_0$ and $Re_0 = 11$; $sp_0 = 3.8d_0$ and $Re_0 = 45$ [42].

6. Use of the super-scalar

An integral solution [68] has been found to apply to liquid fuel combustion for a wide range of configurations: isolated droplet burning, droplet array burning, liquid film burning, or liquid stream burning; steady, quasi-steady, or (in some cases) unsteady gas fields; transient or steady liquid thermal conditions; and stagnant, forced-convective or natural-convective gas fields. So, the allowed configurations include sprays and arrays with droplets but are not limited to droplets. The major constraints are one-step chemical kinetics, Fourier heat conduction, Fickian mass diffusion with uniform mass diffusivities for all species, and unitary Lewis number.

It is well known that, under these circumstances, both $h + \nu QY_O$ and $Y_F - \nu Y_O$ are conserved scalars. h,Y_O, and Y_F are the specific enthalpy, oxidizer mass fraction, and fuel vapor mass fraction, respectively. Q and ν are the fuel heating value (energy per unit mass of fuel) and the fuel-to-air mass stoichiometric ratio, respectively. Each scalar satisfies the same homogeneous advective-diffusive partial differential equation. Therefore, a linear combination of the two conserved scalars will satisfy the same partial differential equation as the original scalars. Defining S as the linear combination named the super-scalar and C as a constant to be determined by the boundary conditions, we have

$$S = h + \nu Y_O + C(Y_F - \nu Y_O) \tag{36}$$

We will consider the case with sufficiently rapid chemical kinetics so that no oxygen reaches the neighborhood of the liquid–

gas interface. At the gas side of the interface, the normal derivative of the super-scalar becomes

$$\left.\frac{\partial S}{\partial n}\right|_s = \left.\frac{\partial h}{\partial n}\right|_s + C\left.\frac{\partial Y_F}{\partial n}\right|_s \tag{37}$$

where n is a normal coordinate at the interface and the subscript s indicates a value at the liquid surface. Via energy-flux balance across the interface, the normal derivative of the enthalpy at the interface is the product of the vaporization mass flux per unit area and L_{eff} divided by ρD. L_{eff} is the energy flux per unit mass flux transferred to the liquid surface. Via fuel-mass-flux balance across the interface, the normal derivative of Y_F at the interface is the product of the vaporization mass flux per unit area and $(Y_{Fs} - 1)$ divided by ρD. Consequently, choosing $C = L_{eff}/(1 - Y_{Fs})$ makes the normal derivative of S become zero-valued at the interface. Note that this requires the special conditions that L_{eff} and Y_{Fs} are uniformly valued along the interfaces.

With a zero-valued normal derivative at any point on the interface and a particular uniformly constant value of the super-scalar S_∞ at infinity, the solution becomes $S = S_\infty$ everywhere in the domain. This is the advantage of the super-scalar over the original conserved scalars which vary through the domain. In particular, the super-scalar S is contrived and shown after integration of the governing equations to be uniform (but possibly time-varying) over the gas field.

$$\begin{aligned} S &= h + \nu\left[Q - \frac{L_{eff}}{1 - Y_{Fs}}\right]Y_O + \frac{L_{eff}}{1 - Y_{Fs}}Y_F = S_\infty \\ &= h_\infty + \nu\left[Q - \frac{L_{eff}}{1 - Y_{Fs}}\right]Y_{O\infty} \end{aligned} \tag{38}$$

It is seen that the value of S can be determined from boundary values without a need to engage the continuity and momentum equations. At the thin flame, the values of Y_F and Y_O become zero. Therefore, the flame temperature T_f is determined by

$$h\left(T_f\right) = S_\infty = h_\infty + \nu\left[Q - \frac{L_{eff}}{1 - Y_{Fs}}\right]Y_{O\infty} \tag{39}$$

Through the phase-equilibrium condition at the interface, Y_{Fs} is known as a function of surface temperature T_s. Thus, T_f is known as a function of the surface temperature, ambient conditions, fuel properties, and L_{eff}. That is, S, T_f, and T_s can be shown to depend on the hydrodynamics, transport phenomena, and geometrical configurations only through L_{eff} and are readily calculable through knowledge of L_{eff} and the prescribed boundary conditions. One may either prescribe the values of T_s and L_{eff} in some rational manner for a special case or couple the transient heating analysis of the liquid interior with this gas-phase analysis to determine T_s and L_{eff}. An example of a special case would be the situation where the wet-bulb surface temperature has been reached with no further heating of the liquid interior. In that case, $L_{eff} = L$, the latent heat for fuel vaporization, and the wet-bulb value for T_s is determined using the super-scalar together with phase equilibrium evaluated at the interface to develop a transcendental algebraic equation for T_s:

$$h(T_s) + \frac{L}{1 - Y_{Fs}(T_s)}Y_{Fs}(T_s) = h_\infty + \nu\left[Q - \frac{L}{1 - Y_{Fs}(T_s)}\right]Y_{O\infty} \tag{40}$$

Variations in the form of the super-scalar are discussed for the cases of multicomponent liquid fuels and vaporization without burning. Comparisons of these results with a few previous results in certain classical configurations can validate the super-scalar. Extensions to other configurations are possible and helpful. For example, the use of the super-scalar to validate sub-grid modeling for laminar and turbulent spray combustion is an attractive possibility.

Certain theoretical problems in fluid mechanics, transport science, and combustion science have been simplified by constructing new variables via linear combinations of the primitive variables. Busemann and Crocco (see Ref. [69]) each accomplished this task for compressible boundary layers by creating new variables from linear combinations of thermal and mechanical variables. These new dependent variables were constant over the boundary layer under certain conditions. This immediately accomplished the integration of a partial differential equation and produced an algebraic relationship connecting the primitive variables. The Shvab-Zel'dovich variables [70] have accomplished the same purpose in many combustion problems. In constructing the new super-scalar as a linear combination of three other scalar quantities, some challenging terms are eliminated in the governing partial differential equations: e.g., viscous dissipation in the boundary layer equations and chemical kinetics in the combustion flow equations. These contrived dependent variables can have constant solutions typically in situations where the boundary conditions involve a uniform value of the variable or a zero value for the normal gradient of the variable over the boundaries. The premixed laminar flame is a problem where the Shvab-Zel'dovich variable can be constant under certain assumptions concerning transport and chemical kinetics. However, in many other combustion problems, the Shvab-Zel'dovich variables vary through space and are not as powerful as a contrivance. The super-scalar S becomes uniform over the space for a wide range of configurations including isolated fuel-droplet burning, droplet-array combustion, group combustion, spray burning, pool burning, and liquid-fuel-film combustion. Here, the Shvab-Zel'dovich variables are conserved scalars but not passive scalars [70]. That is, they are not created or destroyed by chemical reaction terms but do affect velocity fields. The newly contrived super-variable is more than a conserved scalar; it is a uniform scalar of the Crocco-Busemann type. It can have a uniform value in a non-uniform velocity field. The name "super-scalar" (or "super-variable") is given here to distinguish it as more than a conserved scalar.

Consider the gas phase that surrounds or adjoins liquid-fuel droplets, films, pools, and/or streams. Laminar multicomponent flows with viscosity, Fourier heat conduction, Fickian mass diffusion, and one-step oxidation kinetics are analyzed. Mass diffusivities for all species are assumed identical; the Lewis number value is unity; radiation will be neglected; and kinetic energy is neglected in comparison to thermal energy so that, with regard to the energetics, pressure is considered uniform over the space although the pressure gradient can be significant in the momentum balance (small Mach number). Both steady and unsteady scenarios are discussed. The roles of the gas-phase energy equation and the species equations are emphasized. Of course, they must be coupled with the continuity and momentum equations and with a gas equation of state. In addition, the solution of conservation equations for the liquid phase might be required.

The uniformity of the super-scalar S over the gas-phase does require that $L_{eff} = L + \dot{q}_l/\dot{m}$ is instantaneously uniform over liquid surface. The latent heat of vaporization L is a fuel property and therefore will be uniform and constant. The uniformity of the heat flux to the interior per unit mass flux $\dot{q}_l/\dot{m}$ is a more demanding requirement. It can be satisfied in various situations. For example, if the wet-bulb temperature has been reached, $\dot{q}_l = 0$. When a quasi-steady thermal layer exists in the liquid near the surface, $\dot{q}_l/\dot{m} = c_l(T_s - T_o)$ where c_l is the liquid specific heat and T_o is the liquid interior temperature. Then, L_{eff} has a uniform value. In various cases with certain symmetries, $\dot{q}_l/\dot{m}$ can be uniform. In cases where the liquid thermal layer is unsteady, $\dot{q}_l/\dot{m}$ can still be

approximately uniform if the liquid thermal layer thickness is small compared to liquid dimensions (e.g., surface radius of curvature, droplet diameter, pool depth, or film thickness).

The knowledge of the boundary conditions on the gas phase allows also the determination of the B, the Spalding transfer number.

$$B = \frac{h_\infty - h_s + \nu Q Y_{O\infty}}{L_{eff}} = \frac{Y_{Fs} - Y_{F\infty} + \nu Y_{O\infty}}{1 - Y_{FS}} \tag{41}$$

For the spray flow under the conditions cited, the uniform solution for S can be used together with a phase-equilibrium relation to calculate the instantaneous value of the droplet surface temperature. Furthermore, the limiting flame temperature can be determined using Eq. (38). These temperatures depend upon the geometrical configuration or the flow field and flame location only through L_{eff}. These same surface temperature and flame temperature results apply to all configurations (isolated droplets, droplet arrays, droplet groups, sprays, pools, and liquid films) and to steady, quasi-steady, and (for constant or slowly-varying surface temperature) unsteady gas fields whether the liquid interior behaves in a steady, quasi-steady, or unsteady manner. Practically, prior methods of calculation for liquid surface temperature and limiting flame temperature that were complex in even the simplest configurations can be replaced by a method that is simple in the most complex of configurations. Philosophically, the burning of liquid fuels in a wide range of configurations has been unified. The same method applies to the special case of vaporization without burning. For this vaporization case, it applies for multicomponent liquids.

The super-scalar has several possible uses in analysis of liquid-fuel burning. A model for the vaporization and burning of large numbers of fuel droplets must meet the test of producing a uniform value for S under certain specified conditions. In spray computations, it is appropriate to replace one of the dependent variables by S. Even if Le is not unitary, variations in the S variable should be smaller than variations in the primitive dependent variables. The equations presented here apply to laminar flows and to turbulent flows resolved to a scale below the smallest eddy but larger than the average spacing between neighboring droplets. Therefore, any sub-grid turbulence model must allow for the existence of the uniform value solution for the super-variable in the prescribed limits. So, the fidelity of two-phase turbulent reacting flow models can be tested using this criterion.

7. Turbulent combustion of fuel droplet arrays

Turbulent combustion in liquid-fueled continuous combustors is an important issue for researchers and engineers that offers many fundamental research challenges. There are some important scientific questions waiting to be addressed in a proper manner. What role do droplets have for flameholding with turbulent spray flames? What type of individual droplet flamelet structure dominates in various parameter domains: wake flamelet versus envelope flamelet? What type of overall spray flame structure dominates in various parameter domains: individual flamelet versus group flame? Where in the field and when do the droplet flamelets exist as diffusion flames? Fuel-rich premixed flames? Fuel-lean premixed flames? How does the flame structure and location change during the droplets' lifetimes? How do burning rates vary with the turbulence characteristics: e.g., intensity, integral scale, Kolmogorov scale? How do vaporization rates vary with the turbulence characteristics: e.g., intensity, integral scale, Kolmogorov scale? What distortions and modifications occur in the vorticity and turbulence kinetic energy fields due to interactions between droplets and vortex structures of comparable sizes? What are the global effects on chemical conversion rates for mass and energy and therefore on combustor performance? And, the most neglected question of all, how does the turbulence change because of the combustion processes? Obviously, none of these vital questions can be answered by studying domains with only premixed turbulent flames which is where most turbulent combustion research focuses, often under the pretense of relevance to liquid-fueled combustors. With regard to the lean-combustion configuration, if complete vaporization and gas-phase mixing is to be accomplished in a pre-chamber, some of the questions above still are relevant. If complete pre-vaporization and pre-mixing do not result, all of the questions have relevance.

Much of the current research work addresses turbulent combustion in a premixed gas or gaseous turbulent diffusion flames. This single-phase turbulent combustion is an important and interesting fundamental research problem; however, it is the wrong fundamental problem for creating the knowledge base for next-generation power and propulsion solutions that rely on direct injection of liquid fuel. The above scientific questions will not get answered properly. The relevant fundamental problem—liquid spray turbulent combustion — is even more interesting and more challenging but is not being well addressed in the required fundamental fashion.

The presence of liquid fuels sprayed into the combustor changes both the flame structure and the turbulence field; so, the treatment of premixed turbulent flames is not a stepping stone to the treatment of the relevant multiphase non-premixed combustion research problem. The significant differences are (1) the energy spectrum of the turbulence is significantly modified by the presence of droplets; (2) the spray droplets serve as moving flameholders; (3) because of varying local mixture ratio, the flamelets are a combination of diffusion flames and edge flames with fuel-lean, fuel rich, and diffusion-flame branches; and (4) the overall conversion rates for vaporization, chemical compositional change, and chemical energy release and therefore the combustor performance are commonly controlled by processes related to the two-phase character of the reacting flow. There is no reason to believe that useful conclusions about the details of the combustion process in a liquid-fueled continuous combustor will be well approximated by a premixed-gas-flame or gaseous-diffusion flame assumption. For example, it is well known that one should not approximate a laminar spray flame by a premixed gas flame; yet, because of the complexity of turbulence, the analogy of this obviously poor approximation stands without comment for many turbulent flame studies.

The description above pertains to the “rich-burn” design of combustors which is the conventional approach to minimize the formation of oxides of nitrogen by first burning a rich heterogeneous mixture; then adding air to obtain quickly an overall lean mixture. This avoids significant residence time under near-stoichiometric conditions where nitrogen oxides form at the greatest rate. Another strategy which could gain more favor in the future is the “lean-combustion” design. See Dunn-Rankin [71] for an overview of that topic. There, pre-vaporization and pre-mixing of the liquid fuel and air occurs in a separate enclosure before entering the combustor. The same question applies about modification of the spectrum of the turbulence kinetic energy for the heterogeneous mixture. Also, the concern about the effect of turbulence on the mass vaporization rate applies in that case. In addition, the “lean-combustion” concept relies on the ability to mix well in the pre-chamber and have very small compositional (i.e., mixture-ratio) gradients entering the combustor. The interaction amongst the two phases and the turbulence can have significant effects on the uniformity of the mixture ratio and the spectrum of turbulence kinetic energy exiting the pre-chamber and entering

the combustor. We cannot assume that turbulent mixing of the initially heterogeneous mixture follows the same rate laws as turbulent mixing of pure gases. So, lean-combustion has several common issues with rich-burn design to be resolved. Therefore, this proposed research would address the fundamentals of turbulent sprays for both rich-burn and lean-combustion designs.

Karpetis and Gomez [72] conducted an experimental study of a well defined spray flame showing the appearance of combustion in group fashion. Clear indications of two-way coupling in terms of momentum exchange occurred in regions of high liquid-mass loading. A corrugated flame structure developed and advanced downstream to separate "islands" of burning droplet groups.

The goal of a dense array study for droplets in a turbulent flow should be to predict the actual transport rates and vaporization rate for the droplet without having to input laws taken from isolated droplet theory. At this date, such a study does not exist. However, some useful background information is provided in the following subsections.

7.1. Vortex interactions with droplets and sprays

There have been many studies examining vortex–spray interactions where point sources were used to represent droplets, implicitly making both vortex size and spacing between droplets much larger than the droplet size. That is, even, if the droplet had a larger nominal size, its interaction with the vortex or with neighboring droplets is not reflective of the nominal size. The describing laws for vaporization, heating, and drag force are typically input using isolated droplet theory. Nevertheless, although this approach cannot be considered as array theory or serve the purpose of array theory in properly predicting droplet interactions with each other and with turbulent eddies, there are some interesting findings.

Rangel [73] used the vortex dynamics method to consider heat transfer and vaporization of the droplets as well as dispersion. The larger droplets tended to be less sensitive to the vortical structure on account of their higher inertia. The smaller droplets were more easily entrained but tended to vaporize completely before vortex pairing had a significant effect. The droplet properties were calculated by Lagrangian discrete-particle methodology. Rangel and Continillo [74] considered vaporization and ignition for the two-dimensional interaction of a viscous line vortex with a fuel-droplet ring or cloud. The effects of chemical kinetic and vaporization parameters on the ignition-delay time were determined. Aggarwal and co-workers considered the effect of vortex structures on particle-laden flows in several papers [75–77]. The significance of Stokes number on the one-way and two-way particle–vortex interactions was examined. The importance of the preferred-mode frequency for the hydrodynamic instability in defining the Stokes number is discussed.

Bellan and Harstad [78] modeled a cluster of droplets embedded in a vortical structure extending previous studies [79,80]. The cluster and the vortex were assumed to convect together, which differs from the assumption of previous studies. Centrifugal effects caused fuel vapor to accumulate in the vortex core. Harstad and Bellan [81] extended those works to vaporizing polydisperse droplets in an inviscid vortex structure. Each initial-size-class of droplets results in a range of sizes due to the non-uniform environment for the droplets after experiencing centrifuging. So, even in an initially monodisperse spray, a polydisperse spray would result with time. Aggarwal et al. [82] considered a droplet-laden axisymmetric jet with two-way hydrodynamic coupling. The dispersed phase and vaporization had a significant effect on the vortex dynamics. Park et al. [83,84] examined droplet-laden jet undergoing transition. Both evaporating and non-evaporating droplets were considered. The spray was affected by the vortex structures. At high mass loading of the droplets, substantial modification to the vortex dynamics could occur.

Bellan and co-workers addressed jet flows and temporal mixing layers through a range from laminar flows to transitional flows with vaporizing droplets. Miller and Bellan [85] considered a three-dimensional temporally developing mixing layer between two streams, one of which was droplet-laden. Vortex structures formed and the droplets were centrifuged out of the high vorticity regions and migrated to the high strain regions. Abdel-Hameed and Bellan [86] considered laminar jet flows of different cross sections. The presence of drops increases the jet entrainment rate and shortens the core length by an order of magnitude compared to the single-phase jet. The droplet interaction with the flow creates a streamwise vorticity which modifies mixing rates. The circular jet cross-section results in a lower entrainment rate than elliptical, rectangular and triangular cross-sections, similar to the known results for single-phase jets.

The above studies do not detail the flow field around individual droplets and therefore do not determine modification of transport or drag forces due to neighboring droplets. Typically, drag coefficients, Nusselt number, Sherwood number, and vaporization laws are taken from isolated droplet theory. So, they do not fit the definition of array theory. They also do not provide consideration of interactions with vortices that are comparable in size or smaller than the droplet size.

There is some study of interaction between these smaller vortices and an isolated droplet or particle. Kim et al. [87,88] and Masoudi and Sirignano [89–91] examined the interactions between vortices and a droplet or particle of comparable dimension using unsteady, three-dimensional Navier–Stokes flow solvers. Only one paper [91] has accounted for interactions between an isolated vaporizing droplet and comparable-sized vortices. They predicted that significant changes in droplet or particle drag, heating rates, and vaporization rates occur. The vortices are also substantially distorted by the collision with the droplet or particle. Fig. 26 from Masoudi and Sirignano [91] shows the temporal modification of the Sherwood number (and therefore of the vaporization rate) due to the 3D collision of an initially cylindrical vortex with the initially axisymmetric flow around the moving droplet. Five different cases are shown with σ_0, the ratio of initial vortex radius to initial droplet radius, varying from 0.25 to 4.0. Emphasis is placed on vortex size of the same order as the droplet

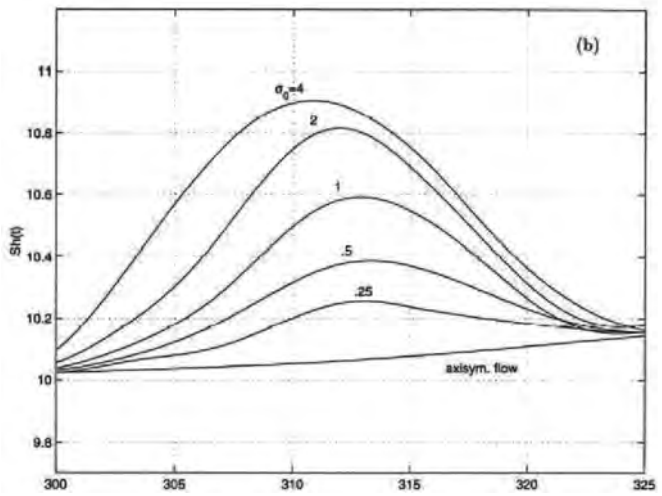

Fig. 26. Changes in Sherwood number of a vaporizing droplet due to collision with a small vortex for various vortex sizes [91].

size because the interaction is more complex there. With very large vortices, the droplet essentially experiences only a changing free stream. The evidence indicates that the collision with one vortex produces substantial change in the behavior.

Repeated collision with many vortices can be expected to produce even greater modifications of the droplet behavior. If a flame existed in the vicinity of the droplet, the fluctuation of the flame by the colliding vortex can be expected to produce even more changes. Not only is the droplet behavior changed but the results show substantial change in the vorticity field at these lower length scales; this result is consistent with the findings of Elghobashi and co-workers which will be discussed later. So, there is evidence that accurate prediction of transport rates and vaporization rates for droplets in vortical flows requires more detailed analysis of the micro-scale behavior. We cannot simply use a vaporization model developed for a flow where small turbulent eddies do not exist.

7.2. Approaches with averaging over shortest length scales

There has been a body of computational research that addresses turbulent spray flows, particle-laden flows, and bubble-laden flows which obviously have the common character of a continuous phase and a discrete phase. A broad review of the topic of vaporizing and burning sprays of liquid fuels can be found in the recent Second Edition of this author's book [1]. In this review paper, only the most relevant literature will be cited. Analyses based on Large-eddy simulations (LES) have been performed. An interesting review of LES for spray flows is presented by Bellan [92]. Note however that LES requires models of sub-grid phenomena; for our cases of interest, the droplet size and average distance between droplets, and the smallest scales of turbulence are all smaller than mesh-size. Consequently, these studies will not provide output that addresses our questions above. Rather, answers are needed to provide good inputs for LES. Sirignano [93,94] identifies some needed inputs.

The LES approach has been used for turbulent particle-laden channel flow by Wang and Squires [95]. Okongò and Bellan [96], Miller and Bellan [97], Leboissetier et al. [98], and Okongò et al. [99] use DNS results to guide development of LES for vaporizing sprays. Some applications of LES for spray combustion were described by Sankaran and Menon [100,101], Menon [102], Menon et al. [103] and Menon and Patel [104].

Okong'o and Bellan [96,105], Leboissetier et al. [98], and Okong'o et al. [99] examine transitional, temporal mixing layers carrying vaporizing droplets. DNS results are generated to provide a database for evaluation of models for LES approaches. Okong'o and Bellan introduced corrections to the filtered variables based on the filtered standard deviation in order to represent the unfiltered variables at the droplet locations for proper calculation of droplet source terms. The LES and DNS compared favorably for global growth of the mixing layer and mixing rates. However, differences were found in dissipation rates and the spatial distribution of the droplets. The filtered droplet source terms were overestimated by the LES. Of course, the LES was shown to be substantially less computationally expensive than DNS.

Vaporization sub-grid models used in spray-combustion and in non-reacting spray flows have not yet accounted for interactions of vortices and vaporizing droplets of comparable dimensions. Some codes have accounted for large eddies interacting with much smaller droplets. Note that the turbulent Reynolds number for flow through a typical gas turbine combustor can be of the order of 10,000 with an integral scale that is tens of centimeters [102–104]. Consequently, the Kolmogorov scale is of the order of 100 microns, which is not much larger than the droplet diameter. Direct numerical simulation (DNS) of turbulent two-phase flows [106] has indicated that the presence of the discrete phase can generate small-scale turbulence. Energy at the end of the turbulent inertial range spectrum has been shown to transfer both to larger particle sizes and to smaller sizes due to the presence of droplets.

There are many analyses described by their authors as direct numerical simulations (DNSs) although that classification is disputable for many of those papers. Often, the presence of the discrete phase is described as a point source in those analyses. So, at best, those studies can only apply to situations where both the average distance between particles, bubbles, or droplets and the size of the smallest turbulence scales are very much larger than the particle, bubble, or droplet size.

In the approaches to the turbulent spray computation, a formal averaging process is made first over at least some, if not all, of the turbulence and spray length scales. For Reynolds-averaged Navier–Stokes (RANS) simulations, averaging is done over all turbulence scales while, for large-eddy simulations (LES), the averaging is done over the smaller scales only. The equations used for two-phase flow often have been developed by averaging over length scales larger than droplet size or distances between neighboring droplets. Consequently, sequential averaging can result in an inability to describe droplet–turbulence interactions properly. A simultaneous rather than sequential averaging is preferred [93]. The averaging must be done after a satisfactory description is made of the turbulence interaction with the vaporizing and burning droplets. That adequate description does not exist and should be a priority for future research.

The challenge for the sub-grid modeling strategy occurs in the situation where the smallest turbulence scales are comparable to or smaller than the droplet and spray scales. Then, the sequential averaging makes no sense. If the averaging for the two-phase flow and the droplet modeling were done first, the smallest scales of turbulence would have been averaged away and should have been included in the droplet model. In this situation, the sequential averaging processes should be replaced by one averaging process that addresses in the sub-grid modeling the droplet behavior, the smallest turbulence scales, and the interaction between the droplets and the turbulence at those sub-grid scales. Such a fundamental approach has not been fully employed. So, existing computations for particle-laden, bubble-laden, and spray flows are only valid for situations where the discrete-particle scales are much smaller than the smallest turbulence scales.

There is a clear need for improved modeling of droplet vaporization in a turbulent, reacting flow as commonly found in many practical applications. For example, in the latest designs of many liquid-fueled, continuous-flow combustors, a rate-controlling process is droplet vaporization. These vaporization rates are very sensitive to instantaneous droplet diameter; relative velocity between the droplet and the averaged gas environment; the turbulence velocity, concentration, and temperature fluctuations in the droplet vicinity; the proximity of neighboring droplets (i.e., droplet number density); the transient droplet heating; and the effect of internal liquid circulation on the transient heating. Although these parameter-sensitivities of the vaporization rate have previously been modeled in some way, there are three major deficiencies that must be corrected before a useful, predictive computational code can be developed. Firstly, these effects must be embodied simultaneously in one model. Current vaporization models typically focus on the physics associated with some sub-set of these parameters. Secondly, the vaporization model must be able to handle a wide and realistic range of turbulence scales for length and time. Thirdly, in order to perform either time-averaged (i.e., Reynolds-averaged Navier–Stokes – RANS- simulations) or large-eddy simulations (LES) of turbulent sprays, a rational two-way coupling must be prescribed between the sub-grid physics and chemistry

and the super-grid physics (i.e., large-eddy fluctuations and mean flow) for both phases. It is important to have some understanding about the dynamic interactions between vortical structures in the surrounding gas and the droplets.

Applications have been confined to situations in which the smallest scale of turbulence is considerably larger than the droplet or the particle size. A few exceptions for flows laden with non-vaporizing solid particles will be discussed below. The interaction between the two phases is modeled by some simplifying equations of the types discussed in earlier chapters. Since velocity gradients on the scales of the droplet diameter and boundary-layer thickness are not resolved, the vorticity generated by means of the droplet–gas interaction are not determined. So, current two-phase DNS is useful only for special classes of turbulent two-phase flows. It cannot be helpful, for example, in evaluating turbulent flow created primarily by a dense spray interacting with a gas.

Masheyak and Pandya [107] reviewed the field of turbulent droplet- and particle-laden flows. Mashayek [108,109] examined spray flows with vaporizing droplets in two flows: a gas flow with stationary (i.e., forced) isotropic turbulence and a turbulent shear flow. The turbulence was artificially forced in the one case so that dissipation would not cause a decrease in intensity. Variable density was allowed at low Mach number but the vapor and surrounding gas were assumed to have the same properties. For the shear flow, vaporization was largest in the region of highest strain rate. Generally, the qualitative behaviors were the expected results; vaporization rate decreased as initial droplet diameter, latent heat of vaporization, boiling temperature, or initial mass loading increased and the rate increased as ambient gas temperature increased.

The current, so-called direct numerical simulation (DNS) approaches for bubble-laden, particle-laden, and spray flows are often not truly direct numerical simulations. Certainly, no studies have true DNS for vaporizing or non-vaporizing spray flows, although we can expect some to be developed in the near future. The currently available studies typically do involve modeling at the droplet (meaning here droplet, solid particle, or bubble) level. That is, the droplet liquid interior and the gas film surrounding each droplet are not resolved. Rather, each droplet is considered as a point with mass and inertia. The aerodynamic forces and heating rates, and vaporization rates are commonly treated through the use of sources and sinks, using algorithms for the source and sink strengths which have been determined through separate analytical or empirical studies; so, they are essentially sub-grid models. Furthermore, these sub-grid models have usually neglected modifications of Nu,Sh,C_D, and C_L through particle interactions with the smallest scales of turbulence.

It is required that we produce DNS models that fully resolve the relevant and interesting length scales for both phases. Earlier, in Section 5, we explained how Wu and Sirignano [40–42,57] and Wu et al. [64] examined three-dimensional laminar flows around vaporizing and burning droplets, using Navier–Stokes solutions for both the liquid interiors and surrounding gas. They showed that, depending on droplet spacing and Damköhler numbers, a variety of configurations could occur. Each droplet could have its own flame or, as spacing decreased, group combustion could occur. At high Damköhler number, the flame could envelop the droplet or group of droplets. At lower Damköhler numbers, the diffusion flame would recede toward the droplet wake forming an edge flame with multiple branches, including fuel-rich premixed flames closer to the vaporizing droplet and fuel-lean premixed flames further from the droplet. We can expect that turbulence will modify some, if not all, of the results. Furthermore, the turbulence will be modified through the expansion and density gradients (baroclinic effect) from heat release and interaction of small eddies with the droplets and the strained flow near the droplets.

The need for better physics-based sub-grid closure for two-phase flows is indicated by the apparent limitations of existing models in characterizing what is observed in actual applications. Issues of interest are the behavior of the spray break-up, droplet dispersion in swirling flow, mixing under different operating conditions. An inherent requirement is that turbulent fine-scale mixing in a two-phase flow be accurately predicted over a wide range of operating conditions without changing the closure models. This was addressed by Menon [102], Menon et al. [103], and Menon and Patel [104]. Attempts to validate existing models have only been partly successful for dilute sprays as well as dense sprays.

A few true DNS calculations for non-vaporizing solid particles in a fluid with decaying isotropic turbulence have been performed. Zhang and Prosperetti [110] developed a numerical method for resolving flows around solid spheres freely moving in a turbulent fluid. Their field contained 100 particles with particle density only 1.02 times the fluid density. Volume fraction was 0.1 and the particle diameter was 8.32 times the initial Kolomogorov scale. Uhlmann [111,112], using an Immersed Boundary Method which applies a force on the fluid at the Lagrangian position of the particle, considered as many as 4096 particles. Using that Immersed Boundary method, Ferrante and Elghobashi [113] and Lucci et al. [114,115] have examined various mass loadings with the solid material density varying from 2.56 to 10 times the fluid density. Up to 6400 particles were considered. The particles increase the dissipation rate and reduce the turbulent kinetic energy, especially at the low wavenumber end of the spectrum because of the large particle sizes.

7.3. Understanding of short-length-scale physics

There is clearly a need for better understanding of the physical and chemical phenomena and interactions on the length scales that relate to the high wavenumber end of the turbulence energy spectrum, droplet sizes, and droplet spacings.

Birouk and Gokalp [116] give a valuable overview of experimental results and correlations for the vaporization of an individual droplet for turbulent environments for cases with zero and non-zero mean-flow relative velocity between the ambient gas and the droplet. For the case with mean-flow, extensions of the Ranz-Marshall and Frossling correlations are presented. In the cases reported, the enhancement of vaporization and heat transport rates by the turbulence depends strongly on the turbulence intensity (i.e., the rms value of the ambient velocity fluctuation) and very weakly on turbulent length scales. However, these experiments are conducted for very large droplet diameters which exceed the smaller turbulence length scales. On the other hand, in typical practical continuous combustors, the droplet sizes are O(100 μm) while the smallest (Kolmogorov) scale is modestly larger. So, existing experiments for interactions of turbulence with vaporizing droplets do not adequately address the relevant question because the relative turbulence scales and droplet scales are not represented. Furthermore, they focus on an individual droplet while the practical configurations involve many droplets interacting with each other and with the turbulent flow. Nevertheless, the correlations can be useful as a benchmark for computations.

Experiments by Dunn-Rankin and co-workers [117,118] have examined vaporizing liquid droplets in a wind tunnel containing an active turbulence generating grid. The tunnel was designed to create turbulence with Kolmogorov scales small relative to the size of the droplets being tested. In order to permit sufficient residence time for measurable evaporation, droplets of heptane were suspended from thin crossed wires. The results for 2 m/s

and 5 m/s mean flows showed that by far the most dominant effect on evaporation comes from the mean flow. For free-flying droplets, the mean flow is much lower, however, and there the effects of turbulence can be expected to be more significant. Even when the droplets are smaller than the Kolmogorov scale, however, the evaporation and mixing of fuel vapor from evaporating droplets will be significantly different in turbulence than in laminar flows.

Although, ultimately, we must address vaporizing and burning droplets, there are some interesting DNS studies for two-phase flows without phase change or chemical reaction. Useful guidance can be obtained. In the classical theory of turbulence for a single-phase fluid, the turbulence kinetic energy is produced only at large scales and then transferred in a cascade fashion to smaller scales with a tendency toward isotropy during the cascade. However, the behavior is substantially different for particle-laden, droplet-laden, and bubble-laden flows. Rather, via interaction with particles, droplets, or bubbles, the turbulence kinetic energy could also be produced on the scale of the discrete elements, e.g., droplets. The newly produced turbulence can be anisotropic. Also, the presence of the discrete phase reduces the Kolmogorov scale. Elghobashi and co-workers have produced vital information and insight here [106,114,115,119–122].

Elghobashi and Truesdell [123] were the first to use direct numerical simulation (DNS) to explain physically how dispersed small particles (with diameter smaller than the Kolmogorov length scale) in decaying isotropic turbulence modify the energy spectrum at all wavenumbers. Ten years later, Ferrante and Elghobashi [106] repeated this study with higher Reynolds number and larger number of particles. In their general case, the particles will change the energy spectrum, turbulence kinetic energy, and its dissipation rate. They showed that a special case exists whereby a particular class of dispersed particles with a specific response time (τ_p) can modify the turbulence energy spectrum at all wavenumbers such that the global turbulence kinetic energy of the particle-laden flow remains equal to that of the flow without particles. The particles in this class were called “ghost particles.” Still, even for this special class, the energy spectrum differs from the case without particles. Temporal changes in turbulence kinetic energy and its dissipation rate are shown in Figs. 27 and 28.

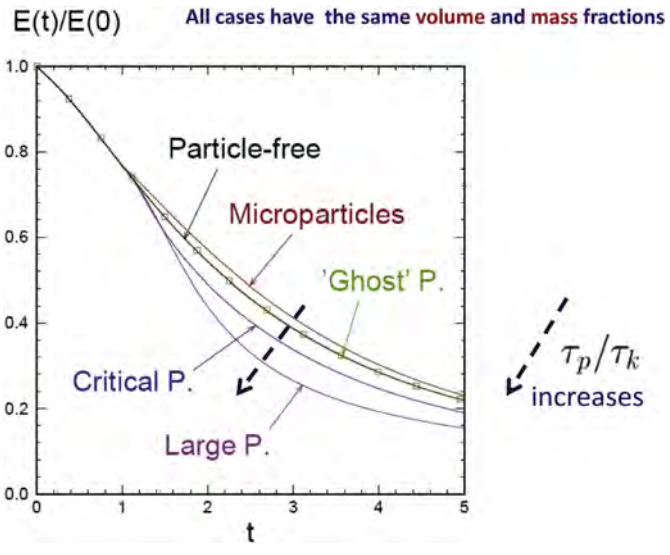

Fig. 27. Temporal variation of turbulence kinetic energy in particle-laden flows. Effect of particle size. [126].

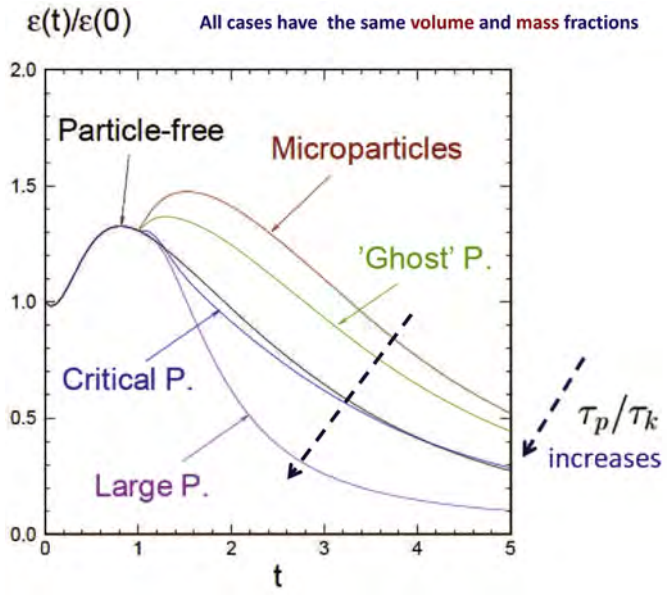

Fig. 28. Temporal variation of turbulence kinetic energy dissipation rate in particle-laden flow. Effect of particle size. [126].

Ahmed and Elghobashi [124] performed the first DNS of particle-laden homogeneous shear turbulent flow and explained how particles with diameter smaller than the Kolmogorov length scale modify the alignment of the semi-longitudinal, counter-rotating, vortical structures in such a way as to reduce the Reynolds shear stresses and hence lower the production rate of turbulence kinetic energy. Note that production of turbulence kinetic energy is a large-scale phenomenon. Lucci, Ferrante and Elghobashi [114] were the first to perform DNS that fully resolves the motion around each of the more than 6000 spherical particles freely moving in decaying isotropic turbulence. In other words, this study does not use the "point particle" model. The results provide physical insight into the two-way interactions between the particles and turbulence. Lucci, Ferrante and Elghobashi [115] were the first to show that the conventional Stokes number (i.e., the ratio of particle response time to the Kolmogorov time scale, τ_p/τ_k should not be used as an indicator for the modulation of turbulence by particles whose diameter is larger than the Kolmogorov length scale.

Elghobashi [125] produced the first map that classified the effects of small particles on turbulence as functions of volumetric loading and response time of the particles. He identified the various distinct physical domains in the parameter space. The term “four-way coupling” was coined in that paper to describe fluid-particle and particle–particle interactions that occur simultaneously in dense suspensions of particles in a turbulent flow. Fig. 29 shows the updated map [126] which include the results of Ferrante and Elghobashi.

In particular, Fig. 29 shows the domains of various types of coupling between the phases. The two parameters in the map are the ratio of the droplet dynamic response time τ_p to the Kolmogorov time scale for turbulence τ_K, and the volume fraction of particles. The Kolmogorov scale is the shortest time scale in the turbulence-kinetic-energy spectrum. The time ratio is plotted on the ordinate while the volume fraction is plotted on the abscissa. Volume fraction is immediately determined from the cube of the ratio of average distance between neighboring particles to the particle diameter (for spheres) or equivalently the product of the number of particles times particle volume divided by the fluid volume. Small normalized distances between neighboring particles

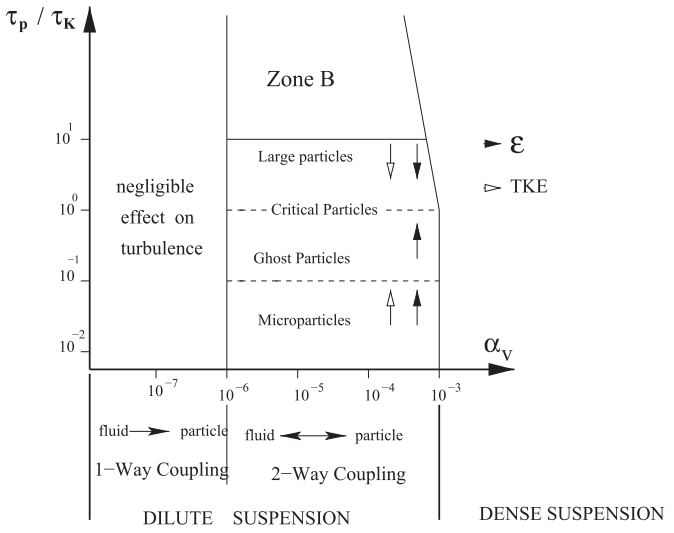

Fig. 29. Elghobashi map of parameter domains for turbulent particle-laden flows [126].

indicate a dense spray or suspension while larger distances result in a dilute condition. There are certain implications for sprays; e.g., for a very dilute spray whereby volume fraction θ is $O(10^{-7} - 10^{-6})$, momentum transfer between the gas and the droplets is important from the droplet perspective; the impact of the momentum transfer on the gas is negligible. This situation is described as a one-way coupling. As the spray becomes less dilute, momentum transfer between the phases is significant for both phases, and we describe this domain as two-way coupling. In Zone B of the figure, higher Reynolds number and slow droplet or particle response (large τ_p) occur and turbulence production is enhanced by the droplets. Higher Reynolds number can result in vortex shedding in the droplet wake. Note though that the higher Reynolds number can be accompanied by higher Weber number which results in droplet breakup leading to smaller droplets and with lower Reynolds number.

Zone A of the figure is divided into four portions by Elghobashi according to the results of certain direct numerical simulations (DNS): large particles $\tau_p/\tau_K > 1$; critical particles $\tau_p/\tau_K = O(1)$; ghost particles $\tau_p/\tau_K < 1$; and micro-particles $\tau_p/\tau_K \ll 1$. In the large-particle regime, both turbulence kinetic energy k and turbulence dissipation rate ε are reduced relative to the single-phase flow. In the critical-particle domain, k is reduced but ε remains about the same relative to a particle-free flow. For the ghost particle domain, k remains about the same but ε is increased relative to a particle-free flow. Both k and ε are increased relative to a particle-free flow in the micro-particle domain.

As the figure shows, very dense sprays with volume fraction $\geq O(10^{-3})$ yield a four-way coupling situation in which, in addition to the two-way coupling characteristics, the droplets or particles exchange momentum directly with neighboring droplets or particles because of collisions (including near collisions that result in the interaction of boundary layers and wakes).

7.4. Summary comments on turbulent spray combustion

It is clear from these existing studies that nothing as simple as a premixed flame or as a set of premixed flames could represent the structure of this burning spray flow. The flames are clearly being held by the droplets; the flame configurations are determined by the droplet array and spacing; the distinction between diffusion flame, fuel-rich premixed flame, and fuel-lean premixed flame depended on Damköhler number and flame location relative to the droplet; and all three types of flames could exist together, either around an individual droplet or around a group of droplets.

Schemes that include averaging over shorter length scales should have a unified averaging process for spray length scales and turbulence length scales. Practical interest for most combustors involves situations where initial droplet size and the smallest turbulent are of the same order of magnitude. Analyses on vaporizing and burning fuel arrays in that domain are needed. Good experimental data in the same domain revealing information on the microscale is greatly needed also. True DNS studies on vaporizing and burning arrays of droplets are needed. These can be developed with the goal of providing useful sub-grid models for LES calculations.

The literature shows for non-vaporizing, non-burning, turbulent, two-phase flows shows that the turbulence energy spectrum, turbulence kinetic energy production and dissipation are significantly modified by the presence of the discrete phase. It is only reasonable to expect similar consequence for spray combustion.

The spray droplets can serve as moving flameholders. The flamelets are a combination of diffusion flames and edge flames. Also, the essential physics governing the flame structure should not be strongly dependent on the detail of the kinetics; the transport, fluid dynamics, and overall reaction time appear to be the governing factors. The turbulence can strongly affect the droplet vaporization while the exchange of mass, momentum, and energy can be expected to affect the character of the turbulence.

References

[1] Sirignano WA. Fluid dynamics and transport of droplets and sprays. 2nd ed. New York: Cambridge University Press; 2010.
[2] Chigier NA, McCreath CG. Combustion of droplets in sprays. Acta Astronaut 1974;1:687–710.
[3] Candel S, Lacas F, Darabiha N, Rolon J-C. Group combustion in spray flames. Multiph Sci Technol 1999;11(1):1–18.
[4] Sirignano WA. Fuel droplet vaporization and spray combustion theory. Prog Energy Combust Sci 1983;9:291–322.
[5] Suzuki T, Chiu HH. Multi-droplet combustion of liquid propellants. In: Proceedings of the Ninth International symposium on space technology and science; 1971.
[6] Chiu HH, Liu TM. Group combustion of liquid droplets. Combust Sci Technol 1977;17:127–42.
[7] Chiu HH, Kim HY, Croke EJ. Internal group combustion of liquid droplets. In: Nineteenth symposium (International) on combustion/the combustion Institute, vol. 19; 1982. pp. 971–80.
[8] Polymeropoulos CE. Flame propagation in a one-dimensional liquid fuel spray. Combust Sci Technol 1974;35:197–207.
[9] Dukowicz JK. A particle-fluid numerical model for liquid sprays. J Comput Phys 1980;35:229–53.
[10] Seth B, Aggarwal SK, Sirignano WA. Flame propagation in a one-dimensional liquid fuel spray. Combust Flame 1978;32:257–70.
[11] Aggarwal SK, Tong AY, Sirignano WA. A comparison of vaporization models in spray calculations. AIAA J 1984;22:1448–57.
[12] Aggarwal SK, Sirignano WA. Numerical modeling of one-dimensional enclosed homogeneous and heterogeneous deflagrations. Comput Fluids 1984;12:145–58.
[13] Aggarwal SK, Sirignano WA. Ignition of fuel sprays: deterministic calculations for idealized droplet arrays. In: Proceedings of the Twentieth Symposium (International) on combustion; 1985. pp. 1773–80.
[14] Aggarwal SK, Sirignano WA. Unsteady spray flame propagation in a closed volume. Combust Flame 1985;62:69–84.
[15] Aggarwal SK, Sirignano WA. An ignition study of polydisperse sprays. Combust Sci Technol 1986;46:189–200.
[16] Annamalai K, Ryan WI. Interactive processes in gasification and combustion. part I: liquid drop arrays and clouds. Prog Energy Combust Sci 1992;18:221–95.
[17] Twardus EM, Brzustowski TA. The interaction between two burning fuel droplets. In: Fifth International Symposium on combustion processes, vol. 8; 1977. Krakow, Poland.
[18] Brzustowski TA, Twardus EM, Wojcicki S, Sobiesiak A. Interaction of two burning fuel droplets of arbitrary size. AIAA J 1979;17:1234–42.
[19] Labowsky M. The effects of nearest neighbor interactions on the evaporation rate of cloud particles. Chem Eng Sci 1976;31:803–13.
[20] Labowsky M. A formalism for calculating the evaporation rates of rapidly evaporating interacting particles. Combust Sci Technol 1978;18:145–51.
[21] Labowsky M. Calculation of the burning rates of interacting fuel droplets. Combust Sci Technol 1980;22:217–26.

[22] Umemura A, Ogawa S, Oshima N. Analysis of the interaction between two burning droplets. Combust Flame 1981;41:45–55.
[23] Umemura A, Ogawa S, Oshima N. Analysis of the interaction between two burning fuel droplets with different sizes. Combust Flame 1981;43:111–9.
[24] Umemura A. Interactive droplet vaporization and combustion approach from asymptotics. Prog Energy Combust Sci 1994;20:325–72.
[25] Tal R, Sirignano WA. Cylindrical cell model for the hydrodynamics of particle assemblages at intermediate Reynolds numbers. AIChE J 1982;28:233–7.
[26] Tal R, Lee DN, Sirignano WA. Hydrodynamics and heat transfer in sphere assemblages-cylindrical cell models. Int J Heat Mass Transfer 1983;26:1265–73.
[27] Tal R, Lee DN, Sirignano WA. Periodic solutions of heat transfer for flow through a periodic assemblage of spheres. Int J Heat Mass Transfer 1984;27:1414–7.
[28] Tal R, Lee DN, Sirignano WA. Heat and momentum transfer around a pair of spheres in viscous flow. Int J Heat Mass Transfer 1984;27:1953–62.
[29] Raju MS, Sirignano WA. Interaction between two vaporizing droplets in an intermediate-Reynolds-number flow. Phys Fluids 1990;2:1780–96.
[30] Chiang CH, Sirignano WA. Interacting, convecting, vaporizing fuel droplets with variable properties. Int J Heat Mass Transfer 1993;36:875–86.
[31] Chiang CH, Sirignano WA. Axisymmetric calculations of three-droplet interactions. Atomization Sprays 1993;3:91–107.
[32] Kim I, Elghobashi S, Sirignano WA. Three-dimensional flow over two spheres placed side by side. J Fluid Mech 1993;246:465–88.
[33] Stapf P, Dwyer HA, Maly RR. A group combustion model for treating reactive sprays in i.c. engines. In: Twenty-seventh symposium (International) on combustion/the combustion Institute; 1988. pp. 1857–64.
[34] Dwyer HA, Stapf P, Maly RR. Unsteady vaporization and ignition of a three-dimensional droplet array. Combust Flame 2000;121:181–94.
[35] Imaoka RT, Sirignano WA. Vaporization and combustion in three-dimensional droplet arrays. Proc Combust Inst 2005;30:1981–9.
[36] Imaoka RT, Sirignano WA. A generalized analysis for liquid-fuel vaporization and burning. Int J Heat Mass Transfer 2005;48:4342–53.
[37] Imaoka RT, Sirignano WA. Transient vaporization and burning in dense droplet arrays. Int J Heat Mass Transfer 2005;48:4354–66.
[38] Sirignano WA, Wu G. Multicomponent-liquid-fuel vaporization with complex configuration. Int J Heat Mass Transfer 2008;51:4759–74.
[39] Sirignano WA. Liquid-fuel burning with non-unitary Lewis number. Combust Flame 2007;148:177–86.
[40] Wu G, Sirignano WA. Transient convective burning of a periodic fuel-droplet array. Proc Combust Inst 2011;33:2109–16.
[41] Wu G, Sirignano WA. Transient convective burning of interactive fuel droplets in single-layer arrays. Combust Theory Model 2011;15:227–43.
[42] Wu G, Sirignano WA. Transient convective burning of interactive fuel droplets in double-layer arrays. Combust Flame 2011;158:2395–407.
[43] Correa SM, Sichel M. The group combustion of a spherical cloud of monodisperse fuel droplets. In: Proceedings of Nineteenth symposium (International) on combustion; 1983. pp. 981–91.
[44] Labowsky M, Rosner DC. Group combustion of droplets in fuel clouds. I. Quasi-steady predictions. In: Zung JT, editor. Evaporation-combustion of fuels. Advances in chemistry series, vol. 166. ACS; 1978. pp. 215–29.
[45] Samson R, Bedeaux D, Saxton MJ, Deutsch JM. A simple model of fuel spray burning. i. Random sprays. ii. Linear droplet streams. Combust Flame 1978;31:14–24.
[46] Law CK. Unsteady droplet combustion with droplet heating. Combust Flame 1976;26:17–22.
[47] Law CK, Sirignano WA. Unsteady droplet combustion with droplet heating-II: conduction-limit. Combust Flame 1977;28:175–86.
[48] Kobayashi H, Park J, Iwahashi T, Niioka T. Microgravity experiments on flame spread of an n-decane droplet array in a high-pressure environment. Proc Combust Inst 2002;29:2603–10.
[49] Mikami M, Oyagi H, Kojima N, Kikuchi M, Wakashima Y, Yoda S. Microgravity experiments on flame spread along fuel-droplet droplet array using a new droplet-generation technique. Combust Flame 2005;141:241–52.
[50] Asano K, Taniguchi I, Kawahara T. Numerical and experimental approaches to simultaneous evaporation of two adjacent volatile drops. In: Proc. 4th Int. conf. on liquid atomization and spray systems; 1988. pp. 411–8.
[51] Patnaik G. A numerical solution of droplet vaporization with convection. Ph.D. Dissertation. Carnegie-Mellon University. Dept. of Mechanical Engineering; 1986.
[52] Chiang CH, Raju MS, Sirignano WA. Numerical analysis of convecting, vaporizing fuel droplet with variable properties. Int J Heat Mass Transfer 1992;35:1307–24.
[53] Raghavan V, Babu V, Sundararajan T, Natarajan R. Flame shapes and burning rates of spherical fuel particles in a mixed convective environment. Int J Heat Mass Transfer 2005;48:5354–70.
[54] Aouina Y, Maas U. Mathematical modeling of droplet heating, vaporization, and ignition including detailed chemistry. Combust Sci Technol 2001;173:1–23.
[55] Dwyer HA, Aharon I, Shaw BD, Niazmand H. Surface tension influences on methanol droplet vaporization in the presence of water. In: Twenty-sixth symposium (International) on combustion; 1996. pp. 1613–9.
[56] Dwyer HA, Shaw BD, Niazmand H. Droplet/flame interactions including surface tension influences. In: Twenty-seventh symposium (International) on combustion; 1998. pp. 1951–7.
[57] Wu G, Sirignano WA. Transient burning of a convective fuel droplet. Combust Flame 2010;157:970–81.
[58] Pope DN, Gogos G. Numerical simulation of fuel droplet extinction due to forced convection. Combust Flame 2005;142:89–106.
[59] Pope DN, Howard D, Lu K, Gogos G. Combustion of moving droplets and suspended droplets: transient numerical results. AIAA J Themophys Heat Transfer 2005;19:273–81.
[60] Westbrook CK, Dryer FL. Chemical kinetic modeling of hydrocarbon combustion. Prog Energy Combust Sci 1984;10:1–57.
[61] Yaws CL. Chemical properties handbook. McGraw Hill; 1999.
[62] Bretsznajder S. Prediction of transport and other physical properties of fluids. Pergamon Press; 1971.
[63] Reid RC, Prausnitz JM, Sherwood TK. The properties of gases and liquids. 3rd ed. McGraw-Hill; 1977.
[64] Wu G, Sirignano WA, Williams FA. Simulation of transient convective burning of an n-octane droplet using a four-step reduced mechanism. Combust Flame 2011;158:1171–80.
[65] Buckmaster JD. Edge flames. Prog Energy Combust Sci 2002;28:435–75.
[66] Nguyen QV, Rangel RH, Dunn-Rankin D. Measurement and prediction of trajectories and collision of droplets. Int J Multiphase Flow 1991;17:159–77.
[67] Mikami M, Oyagi H, Kojima N, Kikuchi M, Wakashima Y, Yoda S. Microgravity ignition experiment on a droplet array in high-temperature low-speed air flow. Combust Sci Technol 2008;153(1):169–78.
[68] Sirignano WA. A general super-scalar for the combustion of liquid fuels. Proc Combust Inst 2002;29:535–42.
[69] White F. Viscous fluid flow. 2nd ed. New York: McGraw Hill; 1991.
[70] Williams FA. Combustion theory. 2nd ed. Reading, Massachusetts: The Benjamin/Cummings Publishing Company, Inc.; 1985.
[71] Dunn-Rankin D. Lean combustion – technology and control. Academic Press; 2008.
[72] Karpetis AN, Gomez A. An experimental study of well-defined turbulent nonpremixed spray flames. Combust Flame 2000;121:1–23.
[73] Rangel RH. Heat transfer in vortically enhanced mixing of vaporizing droplet sprays. In: Tien CL, editor. Annual review of heat transfer, vol. 4. Hemisphere; 1992. pp. 331–62.
[74] Rangel RH, Continillo G. Theory of vaporization and ignition of a droplet cloud in the field of a vortex. In: Proceedings of the twenty-fourth symposium (International) on combustion. The Combustion Institute; 1992. pp. 1493–501.
[75] Aggarwal SK. Relationship between the stokes number and intrinsic frequencies in particle-laden flows. AIAA J 1994;32(6):1322–5.
[76] Aggarwal SK, Uthuppan J. Particle dispersion enhancement in the near region of a forced jet. J Propuls Power 1999;15(2):266–71.
[77] Uthuppan J, Aggarwal SK, Grinstein FF, Kailasanath K. Particle dispersion in a transitional axisymmetric jet: a numerical simulation. AIAA J 1994;32(10):2004–14.
[78] Bellan J, Harstad K. Evaporation of steadily injected, identical clusters of drops embedded in jet vortices. In: Proceedings of the twenty-fourth symposium (International) on combustion; 1992. Poster Session.
[79] Bellan J, Harstad K. Analysis of the convective evaporation of non-dilute clusters of drops. Int J Heat Mass Transfer 1987;30:125–36.
[80] Bellan J, Harstad K. Turbulence effects during evaporation of drops in clusters. Int J Heat Mass Transfer 1988;31:1655–68.
[81] Harstad K, Bellan J. Behavior of a polydisperse cluster of interacting drops in an inviscid vortex. Int J Multiphase Flow 1997;23(5):899–925.
[82] Aggarwal SK, Park TW, Katta VR. Unsteady spray behavior in a heated jet shear layer: droplet-vortex interactions. Combust Sci Technol 1996;113–114:429–49.
[83] Park TW, Aggarwal SK, Katta VR. A numerical study of droplet–vortex interactions in an evaporating spray. Int J Heat Mass Transfer 1996;39:2205–19.
[84] Park TW, Katta VR, Aggarwal SK. On the dynamics of a two-phase, non-evaporating swirling jet. Int J Multiphase Flow 1998;24:295–317.
[85] Miller RS, Bellan J. Direct numerical simulation of a confined three-dimensional gas mixing layer with one evaporating hydrocarbon-droplet laden stream. J Fluid Mech 1999;384:293–338.
[86] Abdel-Hameed H, Bellan J. Direct numerical simulations of two-phase laminar jet flows with different cross-section injection geometries. Phys Fluids 2002;14(10):3655–74.
[87] Kim I, Elghobashi SE, Sirignano WA. Unsteady flow interactions between an advected cylindrical vortex tube and a spherical particle. J Fluid Mech 1995;288:123–55.
[88] Kim I, Elghobashi SE, Sirignano WA. Unsteady flow interactions between a pair of advected vortex tubes and a rigid sphere. Int J Multiphase Flow 1997;23(1):1–23.
[89] Masoudi M, Sirignano WA. The influence of an advecting vortex on the heat transfer to a liquid droplet. Int J Heat Mass Transfer 1997;40(15):3663–73.
[90] Masoudi M, Sirignano WA. Vortex interaction with a translating sphere in a stratified temperature field. Int J Heat Mass Transfer 1998;41(17):2639–52.
[91] Masoudi M, Sirignano WA. Collision of a vortex with a vaporizing droplet. Int J Multiphase Flow 2000;26:1925–49.
[92] Bellan JR. Perspectives on large eddy simulations for sprays: issues and solutions. Atomization Sprays 2000;10:409–25.
[93] Sirignano WA. Volume averaging for the analysis of turbulent spray flows. Int J Multiphase Flow 2005;31:675–705.

[94] Sirignano WA. Corrigendum to 'Volume averaging for the analysis of turbulent spray flows' [International Journal of Multiphase Flow 31 (2005) 675–705]. Int J Multiphase Flow 2005;31:867.
[95] Wang Q, Squires KD. Large eddy simulation of particle-laden turbulent channel flow. Phys Fluids 1996;8:1207–23.
[96] Okongò N, Bellan J. A priori subgrid analysis of temporal mixing layers with evaporating droplets. Phys Fluids 2000;12(6):1573–91.
[97] Miller RS, Bellan J. Direct numerical simulation and subgrid analysis of a transitional droplet laden mixing layer. Phys Fluids 2000;12(3):650–71.
[98] Leboissetier A, Okongò N, Bellan J. Consistent large eddy simulation of a temporal mixing layer laden with evaporating drops. Part 2: A posteriori modeling. J Fluid Mech 2005;523:37–78.
[99] Okongò N, Leboissetier A, Bellan J. Detailed characteristics of drop-laden mixing layers: LES predictions compared to DNS. Phys Fluids 2008;20:103305.
[100] Sankaran V, Menon S. LES of spray combustion in swirling flows. J Turbul 2002;3(001).
[101] Sankaran V, Menon S. Vorticity-scalar alignments and small-scale structures in swirling spray combustion. Proc Combust Inst 2002;29:577–84.
[102] Menon S. Co emission and combustion dynamics near lean blow-out in gas turbine engines; 2004. ASME Paper, GT2004-53290.
[103] Menon S, Stone C, Patel N. Multi-scale modeling for LES of engineering designs of large-scale combustors; 2004. AIAA preprint, 04-0157.
[104] Menon S, Patel N. Subgrid modeling for LES of spray combustion in large-scale combustors. AIAA J 2006;44:709–23.
[105] Okongò N, Bellan J. Consistent large eddy simulation of a temporal mixing layer laden with evaporating drops. Part 1: Direct numerical simulation, formulation and a priori analysis. J Fluid Mech 2004;499:1–47.
[106] Ferrante A, Elghobashi SE. On the physical mechanisms of two-way coupling in particle-laden isotropic turbulence. Phys Fluids 2003;15:315–29.
[107] Mashayek F, Pandya RVR. Analytical description of particle/droplet-laden turbulent flows. Prog Energy Combust Sci 2000;29:329–78.
[108] Mashayek F. Direct numerical simulation of evaporating droplet dispersion in forced low-Mach-number turbulence. Int J Heat Mass Transf 1998;41:2601–17.
[109] Mashayek F. Droplet-turbulence interactions in a low-Mach-number homogeneous shear two-phase flow. J Fluid Mech 1998;367:163–203.
[110] Zhang DZ, Prosperetti A. A second-order method for three-dimensional particle dispersions. J Comput Phys 2005;210:292–324.
[111] Uhlmann M. An immersed boundary method with direct forcing for the simulation of particulate flows. J Comput Phys 2005;209:448–76.
[112] Uhlmann M. Investigating turbulent particulate channel flow with interface-resolved dns. In: International conference on multiphase flow; July, 2007.
[113] Ferrante A, Elghobashi SE. On the effects of finite-size particles on decaying isotropic turbulence. In: International conference on multiphase flow, July 2007:Leipzig; 2007.
[114] Lucci F, Ferrante A, Elghobashi SE. Modulation of isotropic turbulence by particles of Taylor-length scale size. J Fluid Mech 2010;650:5–55.
[115] Lucci F, Ferrante A, Elghobashi SE. Is stokes number an appropriate indicator of turbulence modulation by large particles? Phys Fluids 2011;23:25101-1–25101-7.
[116] Birouk M, Gökalp I. Current status of droplet evaporation in turbulent flows. Prog Energy Combust Sci 2006;32:408–23.
[117] Marti Duran F. Droplet evaporation in an active turbulence grid wind tunnel. M.S. Thesis. Irvine: University of California; 2012.
[118] Moralo O, Mazo D, Dunn-Rankin D. Effects of mean flow and turbulence on the evaporation of a suspended droplet. In: Proceedings of the Southern California conference on fluid dynamics; 2012.
[119] Ferrante A, Elghobashi SE. On the physical mechanisms of drag reduction in a spatially-developing turbulent boundary layer laden with microbubbles. J Fluid Mech 2004;503:345–55.
[120] Ferrante A, Elghobashi SE. A robust method for generating inflow conditions for direct simulations of spatially-developing turbulent boundary layers. J Comput Phys 2004;198:372–87.
[121] Ferrante A, Elghobashi SE. On the accuracy of the two-fluid formulation in dns of bubble-laden turbulent boundary layers. Phys Fluids 2007;19(045105):1–8.
[122] Ferrante A, Elghobashi SE. On the effects of microbubbles on the Taylor-Green vortex flow. J Fluid Mech 2007;572:145–77.
[123] Elghobashi SE, Truesdell GC. On the two-way interaction between homogeneous turbulence and dispersed solid particles ; part 1: turbulence modification. Phys Fluids 1993;A5:1790–801.
[124] Ahmed AM, Elghobashi SE. On the mechanisms of modifying the structure of turbulent homogeneous shear flows by dispersed particles. Phys Fluids 2000;12:2906–30.
[125] Elghobashi SE. On predicting particle-laden turbulent flows. J Appl Sci Res 1994;52(4):309–29.
[126] Elghobashi SE. An updated classification map of particle-laden turbulent flows. In: Proceedings of IUTAM symposium on computational approaches to multiphase flow. Springer; 2006. pp. 3–10.